Diplomarbeit

The role of neutrophil granulocytes on T cell function in bronchial carcinoma (NSCLC)

eingereicht von

Patrick Gschanes-Schweiger

zur Erlangung des akademischen Grades

Doktor(in) der gesamten Heilkunde

(Dr. med. univ.)

an der

Medizinischen Universität Graz

ausgeführt am

Lehrstuhl für Pharmakologie

unter der Anleitung von

Ass.-Prof. PD Mag. rer. nat. PhD Julia Kargl

Univ.-Prof. Dr. med. univ. Akos Heinemann

Graz, am 11.05.2022

Eidesstattliche Erklärung

Ich erkläre ehrenwörtlich, dass ich die vorliegende Arbeit selbstständig und ohne fremde Hilfe verfasst habe, andere als die angegebenen Quellen nicht verwendet habe und die den benutzten Quellen wörtlich oder inhaltlich entnommenen Stellen als solche kenntlich gemacht habe.

Graz, am 11.05.2022 *Patrick Gschanes-Schweiger eh.*

Acknowledgments

An dieser Stelle möchte ich die Gelegenheit nutzen um mich beim gesamten Team der Arbeitsgruppe Kargl für ihre kollegiale Zusammenarbeit und Hilfsbereitschaft zu bedanken. Namentlich möchte ich Kathrin Maitz, Sofia Raftopoulou, Paulina Valadez Cosmes, Sabine Kern sowie Iris Red und Kathrin Rohrer erwähnt haben, die mich nicht nur in die Methoden der praktischen Laborarbeit eingeführt haben, sondern auch während den gesamten 16 Wochen meiner Laboratoriumszeit stets für Rückfragen bereitstanden und sanftmütig mit mir als Lernenden umgingen – dies lässt sich generell für alle Mitarbeiter des Lehrstuhls für Pharmakologie sagen.

Im Besonderen gilt mein Dank auch an meine Erstbetreuerin, Ass.-Prof. Julia Kargl, die mir mit ihrer duldsamen Art und ihrem Weitblick stets lösungsorientiert zeigte, wie man sich bei den unzähligen Problemstellungen der Grundlagenforschung sukzessive an die Wahrheit herantastet; auch für ihre Geduld und Empathie bis zur definitiven Fertigstellung dieser Arbeit im sechsten Studienjahr sowie für die Begutachtung dieser möchte ich mich bei ihr bedanken. Nicht unerwähnt bleiben dürfen mein Zweitbetreuer, Prof. Akos Heinemann, der als Lehrstuhlinhaber die Materialien und Gerätschaften zur Verfügung stellte und somit die praktische Arbeit erst ermöglichte, sowie Sarah Knights, die diese Arbeit lektorierte.

Des Weiteren möchte ich mich bei meinen Eltern sowie meinen beiden älteren Schwestern für ihre mentale Unterstützung bedanken. Insbesondere während intensiver Arbeitsphasen, welche sich de facto durch das gesamte Studium durchziehen, boten sie mir den nötigen Rückhalt um dieses Studium abzuschließen; man könnte meinen, dass auch sie ihren Beitrag für den Abschluss dieses Studiums leisteten.

Zu guter Letzt gebührt mein Dank auch Isabel, die mir mit ihrer Art in der finalen Phase meines Studiums auch während ernüchternder Momente immer wieder den Weg zur Glückseligkeit zeigte.

Table of contents

Abbreviations and definitions VI
List of figures IX
List of tables XI
Abstract XII
Kurzzusammenfassung XIII
1. Introduction 1
1.1. Non-small cell lung cancer (NSCLC) and treatment approaches 1
1.2. Immune system in general 3
1.2.1. T lymphocytes 4
1.2.2. Antibodies 6
1.2.3. Neutrophil granulocytes 6
1.3. Tumor immunology 7
1.3.1. The role of neutrophils in cancer 9
1.3.2. Neutrophils as therapeutic targets in ICI therapy 11
1.4. Cell analysis by flow cytometry 12
1.4.1. Principles of flow cytometry 12
1.4.2. Immune cells on the screen 14
1.4.3. Identification of immune cell properties 15
2. Hypothesis 17
3. Materials and methods 18
3.1. Blood collection 18
3.1.1. Extraction of cell factions 18
3.1.2. Isolation of T lymphocytes from PBMCs 19
3.1.3. Cell counting 20
3.1.4. Isolation of eosinophil granulocytes from PMNLs 22
3.1.5. Isolation of neutrophil granulocytes from PMNLs 23
3.1.6. Neutrophil shape change assay 23

3.2. Tumor cell culture 24
3.2.1. Cell lines and used ingredients 24
3.2.2. Storage and freeze/thaw procedures 25
3.2.3. Cell collection and splitting of cells 25
3.2.4. Mycoplasma detection test 26
3.2.5. Cell supernatants – seeding, starving and harvesting 26
3.3. T cell proliferation assay 27
3.3.1. T cell mono-culture 27
3.3.2. T cell and neutrophil co-culture 29
3.3.3. T cell staining for flow cytometric analysis 31
3.4. T cell apoptosis assay 32
3.5. Immunostaining for flow cytometry 33
3.5.1. Selection of antibody dyes 33
3.5.2. Limitations of combinations 34
3.5.3. Staining protocol 34
3.6. Measurement and compensation in flow cytometry 40
3.6.1. Preparation 40
3.6.2. The actual measurement 41
3.6.3. Compensation 41
3.7. Software packages 41
3.8. Data processing 41
3.9. Statistics 42
4. Results 43
4.1. Neutrophil activation upon IL-8 stimulation behaved in a similar fashion using naïve neutrophils and neutrophils recovered from the eosinophil isolation protocol 43
4.2. Stain indices from APC and PE topped the ranking, whereas SI from eF450 proliferation dye and FITC as part of apoptosis dye were less bright 44

4.3. Compensation was done properly only, when the median fluorescence of the false-positives was equal to the median fluorescence of the negatives ... 45

4.4. No differences in generation zero of T cells after co-culturing with stimulated neutrophils compared to T cells in mono-culture ... 49

4.5. No differences in apoptosis counts of T cells after co-culturing with stimulated neutrophils compared to T cells in mono-culture ... 53

5. Discussion ... 57

6. References ... 60

Abbreviations and definitions

γδ-T cell	Gamma delta T cell; a subset of intraepithelial lymphocytes
ABAH	4-Aminobenzoic acid hydrazide
ABH	2(S)-amino-6-boronohexanoic acid
ANC	Absolute neutrophil count
APC (introduction)	Antigen presenting cell
APC (material)	Allophycocyanin
ARG1	Arginase 1
BSA	Bovine serum albumin
CD	Cluster of differentiation
CMP	Common myeloid progenitor
CLP	Common lymphoid progenitor
CT	Computed tomography
CTL	Cytotoxic T lymphocyte
CXC	(α-)chemokine; one of four subfamily of chemokines
CXCR	CXC chemokine receptor
CXCL	CXC chemokine ligand
DAPI	4′,6-Diamidin-2-phenylindol
DI water	Deionized water
DMEM	Dulbecco's Modified Eagle's Medium
DMSO	Dimethyl sulfoxide
DPBS	Dulbecco’s phosphate buffered saline
EDTA	Ethylenediamine tetraacetic acid
ELISA	Enzyme-linked immunosorbent assay
FACS	Fluorescence activated cell sorting
FATP2	Fatty acid transport protein 2
FBS	Fetal bovine serum
FGF	Fibroblast growth factor
FITC	Fluorescein
FMO	Fluorochrome minus one
FSC	Forward scatter
FVD	Fixable viability dye
G-CSF	Granulocyte colony-stimulating factor
G/PMN	Granulocytic or polymorphonuclear
Gr1	Granulocyte antigen-1

HBSS	Hanks‘ Balanced Salt Solution
HEPES	N-2-Hydroxyethylpiperazine-N'-2-ethanesulfonic acid
IASLC	International Association for the Study of Lung Cancer
ICAM	Intracellular adhesion molecule 1
IC fixation	Intracellular fixation
ICI	Immune checkpoint inhibitor
IL	Interleukin
iNOS	Inducible nitric oxide synthase
IRS1	Insulin receptor substrate 1
MFI	Mean fluorescence intensity
MHC	Major histocompatibility complex
MMP9	Matrix metalloproteinase 9
NE	Neutrophil elastase
NK cell	Natural killer cell
NSCLC	Non-small cell lung cancer
PBMC	Peripheral blood mononuclear cell
PBS	Phosphate-buffered saline
PCR	Polymerase chain reaction
PD-1	Programmed cell death protein 1
PD-L1	Programmed cell death 1 ligand 1
PE	Phycoerythrin
PE-Cy7	Phycoerythrin/Cyanine7
PerCP-Cy5.5	Peridinin chlorophyll protein-Cyanine5.5
PET-CT	Positron emission tomography – computed tomography
PFA	Paraformaldehyde
PGE2	Prostaglandin E2
PI	Propidium Iodide
PI3K	Phosphatidylinositol-3-kinase
PMNL	Polymorphonuclear cell
PMSF	Phenylmethylsulfonylfluoride
PMT	Photomultiplier tube
PROK2	Prokineticin 2
PS	Penicillin-Streptomycin
RBC	Red blood cell
RNS	Reactive nitrogen species
ROS	Reactive oxygen species

RPMI	Roswell Park Memorial Institute Medium
RT	Room temperature
SB	Staining buffer
SCLC	Small cell lung cancer
SI	Stain index
SSC	Side scatter
TGFß	Transforming growth factor ß
TME	Tumor microenvironment
TNFα	Tumor necrosis factor-α
TNM	Tumor (T), nodes (N), and metastases (M)
TPS	Tumor proportion score
Treg	Regulatory T cell
TSP-1	Thrombospondin-1
UICC	Union for International Cancer Control (UICC)
VEGF-A	Vascular endothelial growth factor-A
WBC	White blood cell
WHO/IARC	World Health Organization / International Agency for Research on Cancer

List of figures

Figure 1: Principle of flow cytometry. 13
Figure 2: Acquisition of data. 14
Figure 3: Depiction of anti-CD3 uncoated sample using univariate and bivariate plots. 15
Figure 4: Quadrant and spider gate. 16
Figure 5: Range gate and bisector gate. 16
Figure 6: Boolean and hierarchical gating. 17
Figure 7: Fractioning of leukocytes using a density gradient. 19
Figure 8: Microscopic view of the NEUBAUER counting chamber. 21
Figure 9: Magnetic isolation of eosinophils. 23
Figure 10: Treatment of neutrophils. 30
Figure 11: Example of conditions in co-culturing of T cells and neutrophils. 31
Figure 12: Algorithm of the in-house established surface antibody staining protocol. 35
Figure 13: Proliferation of T cells detected by eF450 proliferation dye. 36
Figure 14: PI/Annexin V apoptosis dye elicited early and late apoptotic T cells. 39
Figure 15: Identical dose response curves in PMNL and isolated neutrophils upon IL-8 stimulation. 43
Figure 16: Emission overspill and compensation for the FL2 channel. 45
Figure 17: Uncompensated single-color stained sample (FL2 = FL2 – 0% FL1). 46
Figure 18: Undercompensated single-color stained sample (FL2 = FL2 – 30% FL1). 46
Figure 19: Overcompensated single-color stained sample (FL2 = FL2 – 36% FL1). 47
Figure 20: Highly overcompensated single-color stained sample (FL2 = FL2 – 40% FL1). 47
Figure 21: Properly compensated single-color stained sample (FL2 = FL2 – 34.5% FL1). 48
Figure 22: Expected emission spectra of a multicolor panel for proliferation dye and surface antigen staining in T cell proliferation assay 49
Figure 23: Representative compensation matrix of the multicolor panel in the T cell proliferation assay. 50

Figure 24: Flow gating of the multicolor panel in the T cell proliferation assay. 51
Figure 25: Percentages of generation zero in $CD4^+$ and $CD8^+$ T cells at day 3 and day 6. 52
Figure 26: Expected emission spectra of a multicolor panel for apoptosis dye and surface antigen staining in the T cell apoptosis assay. 53
Figure 27: Representative compensation matrix of the multicolor panel in the T cell apoptosis assay. 54
Figure 28: Flow gating of the multicolor panel in the T cell apoptosis assay. 55
Figure 29: Percentages of early and late apoptosis counts in $CD4^+$ and $CD8^+$ T cells. 56

List of tables

Table 1: Recipe for T cell medium for 5 mL. 27
Table 2: Treatment of neutrophils. 30
Table 3: Multicolor sample for surface antigen staining in T cell proliferation assay. 32
Table 4: Multicolor sample for surface antigen staining in T cell apoptosis assay. 33
Table 5: Stain indices from the used fluorophores in the panels. 44

Abstract

Introduction and Objectives: The presence of neutrophil granulocytes in the TME has been repeatedly described. Recent studies of patients with NSCLC have shown that tumor-associated neutrophils (TANs) show a negative correlation with T lymphocytes and have an immunosuppressive effect in which T lymphocytes are inhibited in their function to fight against tumor cells. The aim of this study was to complement existing data, which have verified the promotion of tumor growth by inhibition of $CD8^+$ T cells through TANs, by performing co-culture experiments of human T cells together with neutrophils *in vitro* as part of an experimental setup.

Materials and methods: Blood samples were collected from healthy donors and T cells and neutrophils were isolated for co-culture experiments. T lymphocyte-neutrophil co-cultures were measured after three and six days in a proliferation assay and after 24 hours in an apoptosis assay. Before seeding, naïve neutrophils were treated with supernatants of cell lines either from lung cancer (A549) or normal human bronchial epithelium (B2B) to polarize them towards TANs; for comparison, a negative control of mono-cultured T lymphocytes was performed. After culturing, T cells were stained for CD4 and CD8 to separate T cell subsets and with eF450 proliferation dye for proliferation experiments or with PI/Annexin V apoptosis dye for apoptosis experiments. T cell proliferation and apoptosis were analyzed using flow cytometry. For both assays, four samples under identical experimental conditions were used for statistical analysis.

Results: The co-cultures differed from the negative control only to a small extent. Neither statistically significant differences in proliferation behavior nor in enhanced apoptosis counts in $CD4^+$ or $CD8^+$ T cells could be observed. Co-cultures with A549-treated neutrophils showed the biggest disruption of T lymphocytes in proliferation behavior and in the absolute percentage of apoptosis. Overall, the analysis delivered contradictory results.

Discussion: These observations indicate that the methods are still too immature to substantiate a possible negative correlation between neutrophils and T cells in a human model. Furthermore, the p-value had suffered from low sample size. Particularly paradoxical results may point to necessary improvements in terms of single reagents, experimental setup or work steps.

Kurzzusammenfassung

Einleitung und Ziele: Die Präsenz von neutrophilen Granulozyten im Tumorgewebe wurde mehrfach beschrieben. Aktuelle Studien bei Patient*innen mit NSCLC schreiben den Tumor-assoziierten Neutrophilen (TANs) eine negative Korrelation zu den T-Zellen und die Rolle eines immunsuppressiven Akteures zu, welche die T-Lymphozyten bei ihrer Bekämpfung von Tumorzellen inhibieren. Ziel dieser Studie war es, publizierte Daten, welche die Förderung des Tumorwachstums durch Inhibierung der $CD8^+$ T-Zellen durch TANs bestätigten, durch *in vitro* Ko-Kultivierung von humanen T-Zellen mit Neutrophilen im Rahmen eines Versuchsaufbaus zu untermauern.

Materialien und Methoden: Zur Ko-Kultivierung wurden T-Lymphozyten und neutrophile Granulozyten aus entnommenen Blutproben von gesunden Spender*innen isoliert. Die Ko-Kulturen aus T-Zellen und Neutrophile wurden nach drei und sechs Tagen im Proliferationsassay und nach 24 Stunden im Apoptoseassay ausgewertet. Vor der Zusammenführung wurden naive neutrophile Granulozyten mit Zellüberständen von Zelllinien entweder aus Lungenkarzinom (A549) oder normalem humanen Lungenepithel (B2B) behandelt, um diese zu TANs zu polarisieren; dazu vergleichend wurde eine Negativkontrolle aus monokultivierten T-Zellen angelegt. Nach der Kultivierung wurden die T-Zellen auf CD4 und CD8 zur Unterscheidung der T-Zell-Untergruppen und mit der eF450 Proliferationsfärbung für Proliferationsexperimente oder mit der PI/Annexin V-Apoptosefärbung für Apoptoseexperimente gefärbt. Mittels der Durchflusszytometrie wurden T-Zell-Proliferation und -Apoptose analysiert. Für beide Assays wurden jeweils vier Stichproben unter den gleichen experimentellen Bedingungen zur statistischen Auswertung herangezogen.

Ergebnisse: Die Veränderungen in den Ko-Kulturen waren vergleichsweise zur Negativprobe nur von geringem Ausmaß, sodass weder statistisch signifikante Veränderungen des Proliferationsverhaltens noch statistisch signifikant erhöhte Apoptosezahlen bei CD4 oder CD8 positiven T-Zellen gezeigt werden konnten. Bei jenen Ko-Kulturen mit A549-behandelten neutrophilen Granulozyten konnte man meist die größten Störungen der T-Lymphozyten im Proliferationsverhalten bzw. den höchsten absoluten Prozentanteil in der Apoptose beobachten; insgesamt lieferten die Auswertungen jedoch paradoxe Ergebnisse.

Diskussion: Diese Beobachtungen machen kenntlich, dass die Methoden noch nicht ausgereift waren, um eine mögliche negative Korrelation zwischen neutrophilen Granulozyten und T-Lymphozyten im humanen Modell zu untermauern. Ebenfalls war der Stichprobenumfang relativ niedrig, sodass der p-Wert darunter gelitten hat. Paradoxe Ergebnisse können darauf hinweisen, dass einzelne Reagenzien, Versuchsaufbau oder Arbeitsschritte noch verbessert werden müssen.

1. Introduction

1.1. Non-small cell lung cancer (NSCLC) and treatment approaches

Lung cancer continues to be the most common cause of cancer death (close to 25%) among men and is already the second most common cause of cancer death (16%) with increasing development among women in German-speaking countries in 2016. Of concern is not only the increasing incidence caused by major risk factors of active/passive smoking and various pollutants, but also the limitations in therapy, as clinical symptoms usually occur at an advanced and incurable stage (1-4). Overall, lung cancer appears rather as a disease of the elderly, aged 60 and older (86% in the U.S. in 2015) in conjunction with a very adverse prognosis where the five-year survival rate ranges from 56% in localized disease to 5% in metastatic disease and the one-year-survival rate is gender independently less than 50% after diagnosis (5).

Early-stage lung cancer patients often appear clinically without any signs or symptoms opposed to late-stage lung cancer patients. Symptoms are often unspecific such as coughing, dyspnea, thoracic pain, weight loss, weakness, fever, night sweats and the more specific (but delayed) hemoptysis (2,3).

Owing to the frequent unspecific symptoms, diagnosis is made by synopsis of risk factors (age from 40 upwards together with smoking or long-term exposure to pollution), clinical presentation, laboratory and imaging, where the first choice method is still the computed tomography (CT) of the thorax. When a suspicious region is localized and explanatory for the symptoms, the diagnostic assurance occurs by biopsy with an ensuing histological examination. When lung cancer is histologically confirmed, staging procedures (e.g. PET-CT) are performed, which include the eventual detection of metastases as well (2,3).

Histological classification allows differentiation between small cell lung cancer (SCLC, 15% of lung cancers) and non-small cell lung cancer (NSCLC, 85% of lung cancers), which is subcategorized into adenocarcinoma (40%), squamous cell carcinoma (35%), large cell carcinoma (10%) and a few rare entities (1,2,6). In terms of clinics and therapy, oncologists merely distinguish between the typical

aggressive SCLC, which have in ~80% of cases already seeded metastases at the time of diagnosis, and the more likely resectable NSCLC, which in contrast to SCLC do not respond well to radio- or chemotherapy (1). Overall, therapeutic approaches are still a subject of ongoing studies on combinations of myriad modern chemotherapeutics in conjunction with radio-, immunotherapy and/or surgery. Therapy currently shows disappointing results in the long-term curing of lung cancer but achieves markedly middle-term improvement of the symptoms (1,2).

Patients with NSCLCs are classified after histological classification based on WHO/IARC (7) and staging (imaging) based on the TNM classification (according to IASLC lung cancer staging project) in accordance with the classification of UICC 8 (8). This ranges from stage 0 with carcinoma in situ, as a form of precancer, to stage IVB with multiple metastases and determines the different curative (up to and including stage IIIA) or non-curative/palliative (stage IIIB/C and IV) regimens. For modern chemotherapy, the distinction described above requires patients in stage IV (metastases) to undergo a molecular biological investigation of the biopsy in terms of its mutational load. Besides the staging and traits of the patient (general condition, sex, comorbidities) this determines the individualized treatment (3).

The relatively novel treatment by immunotherapy using immune checkpoint inhibitors (ICI) requires an immune histological investigation. For that, PD-L1 expression in tumor cells is quantified according to tumor proportion score (TPS). In studies ICIs are presently implemented in non-curative settings (stage IIIB and upwards) and mainly in NSCLCs without any genetic aberrations as either monotherapy (when PD-L1 is located on more than 50% of tumor cells) or in combination with chemotherapy. In patients with stage III and undergoing definitive radio-chemotherapy without progressive disease and PD-L1-positive tumor cells, ICIs are also used (3). Moreover, in some studies (e.g. IMpower010 (9)) ICIs are even used as the ensuing consolidation in lower stages (even starting from stage IB upwards). However, the use of those novel therapeutics, including tyrosine kinase inhibitors, is currently not implemented as a default systemic therapy (3).

Studies indicate that the advantage of several ICIs (such as Pembrolizumab, Atezolizumab, Cemiplimab) as monotherapy compared to conventional

chemotherapeutics (containing platinum) on tumors with > 50% PD-L1 expression is a reduction of severe side effects, the extension of progressive-free survival and survival time (10,11). In contrast and independent of PD-L1 expression, the use of chemotherapy in combination with a single ICI is also recommended. Interestingly, the use of two ICIs in combination increases the side effects compared to ICI monotherapy or chemotherapy plus ICI (12-16). With stable disease, there may be a maintenance therapy with ICI monotherapy or chemotherapy plus ICI (RCT studies with Pembrolizumab, Nivolumab, Ipilimumab) (3).

In the past, the selection of ICIs was based on theoretical considerations. A comprehensive molecular profiling of the heterogeneous NSCLC tumors (inter alia from adenocarcinoma, squamous cell carcinoma) and knowledge of strategies from NSCLC of evading immune response by the expression of specific proteins (e.g. PD-1, programmed cell death protein 1 as inhibitory receptor on T lymphocyte and his ligand PD-L1, programmed cell death 1 ligand 1 secreted by tumor cells) exist. However, in the absence of a foundational knowledge of tumor-associated immune cells, the response rate of ICIs merely amounts to ~20% so far (17).

To improve the low response rate of ICI therapy, a better understanding of the interaction between immune and tumor cells located in the now well-understood tumor microenvironment (TME) will be important. This would enable a potential secondary therapeutic strategy to reduce the number of therapy-refractory NSCLC-patients treated with ICIs (18).

1.2. Immune system in general

Within the complexity of the immune system, physicians distinguish between the (unspecific) innate immunity and the (specific) adaptive immunity. The (unspecific) innate immunity is composed of the myeloid system, granulocytes, monocytes, natural killer (NK) cells and dendritic cells. It is responsible for immediate effector functions and is characterized by high turn-over *in vivo*, i.e. for the fast new formation and degradation of cells. The (specific) adaptive immunity harbors T and B lymphocytes, which are equipped with antigen receptors and characterized by

clonal expansion whereby parts of this clonal expansion possess memory function (19).

By using antigen-presenting cells, the adaptive immunity can perform its function of eliminating intruders specifically and achieve homeostasis by clonal proliferation. Dendritic cells are antigen-presenting cells (APC; alongside macrophages and B cells) and can be seen as a bridge between the innate and adaptive immunity. NK cells actually belong to the innate immunity due to their inability to clonal expansion, but in terms of their functionality and by a common lymphatic progenitor cell they are practically assigned to lymphocytes (19,20).

Both the innate and adaptive immune systems emerge from the same (omnipotent) hematopoietic stem cell in the bone marrow. Derived progenitor cells (multipotent to oligopotent) differentiate by the influence of various growth factors into the different immune cells in the tissue, e.g. in secondary lymphatic organs (19). Throughout development, each cell type is characterized by the up- or downregulation of specific receptors. NK cells and B and T cells stem from a common lymphoid progenitor (CLP), whereas the innate immune system, similar to erythrocytes and platelets, stems from a common myeloid progenitor (CMP) and matures to the respective demanded cells (21).

T lymphocytes and neutrophil granulocytes as respective representatives of adaptive and innate immunity against NSCLC are described below. Both are abundantly located in TME of NSCLC (18).

1.2.1. T lymphocytes

As part of the specific immunity, naïve T and B cells can usually be found in the parafollicular cortex of lymph nodes (periphery) where dendritic cells perform antigen presentation (using MHC-II molecules) and secrete cytokines to activate naïve T cells. After activation, the naïve T cells become effector cells, either transforming into cytotoxic T cells ($CD4^-/CD8^+$) or into T helper cells ($CD4^+/CD8^-$) (19).

In case of T helper cells, there are different subsets with different functions, e.g. for supporting B cells in generating antibodies. There is also a subset of regulatory T cells (Tregs), which are capable of inhibiting T cell activation, T cell effector

functions and the modulation of NK cells to prevent them from attacking the body's own cells (19,20).

The cytotoxic T cells ($CD8^+$) cooperate closely with NK cells that use MHC-I molecules for recognizing the body's own nucleated cells. When detecting loss or degradation of the MHC-I molecule in viral infected or neoplastic cells, NK cells initiate attraction of $CD8^+$ cells for attacking and/or take on cell destruction by themselves. However, by perpetual MHC-I expression, some viruses and neoplasms can evade immune response (19).

After clonal expansion and elimination of the antigen (effector phase) the response ceases by apoptosis of the antigen-stimulated effector cells, thereby restoring homeostasis (contraction phase) and sparing a few effector cells ($CD4^+$ and $CD8^+$) to remain memory cells for faster (re-)activation in future infections with the same antigen-presenting microbe (19,20).

Both T and B cells can generate a vast variability of receptors with more than 1×10^7 possibilities by rearrangement of DNA. B cells are capable of rearranging their germline DNA over their whole lifetime, thereby recognizing free antigens (without any support from APCs) and antigen-MHC-complexes. In contrast, mature T cells, which merely recognize antigens using MHC-complexes on the body's own cells (MHC molecules) after undergoing positive selection throughout their development in the thymus. This explains the myriad of T cells with different T cell receptors, which should thrive in the thymus to be stimulated by an appropriate antigen in the periphery. Activation of cytotoxic T lymphocytes (CTL) occurs by processing the antigen in the infected cell by proteasome and lysosomal enzymes into short fragments which are bound to MHC-I proteins (α1 and α2 bind to antigen fragment) and presented to CTL (with α3-binding site) on the cell surface. In contrast, macrophages and B cells use T helper cells for binding an antigen on their MHC-II complex whereby the $CD4^+$ cell reinforces the macrophage/B cell in their function (19).

Meaningful to this study were the different cluster of differentiation (CD) antigens of the T cells in general ($CD3^+$), and of their two ensuing main fractions consisting of T helper cells ($CD4^+/CD8^-$) and cytotoxic T cells ($CD4^-/CD8^+$). CD3 is a non-covalent binding complex and part of the T cell receptor. It works as a chaperone

for signal transduction for newly synthesized T cell receptors to the cell surface. Non-$CD3^+$ cells from PBMCs (chapter 3.1.1.) are represented by B cells, dendritic cells, monocytes and NK cells. This is merely a very small excerpt of the entire CD molecule list, which now comprises up to 350 designations (22,23).

1.2.2. Antibodies

The knowledge and use of antibodies has become one of the most crucial components in modern medicine, not only in the increasing number of targeted therapies (including ICIs) but also their simple use in diagnostics as part of flow cytometry (19).

Secreted by B cells, they are soluble B cell receptors. Antibodies contribute to humoral immunity by neutralizing microbes and toxins by opsonization, lysis, initiating phagocytosis of microbes and antibody-dependent cellular cytotoxicity by binding to Fc receptors. VDJ-recombinations determine the antibody-production in B cells, where each antibody (or even receptors in T cells) is composed of the variable (V), diversity (D) and joining (J) segment. The more precise the punctual mutation in immunoglobulin genes in B lymphocytes, the higher the affinity of the antibody to antigen, hence a survival advantage for those B cells, which produce high-affinity antibodies (19).

1.2.3. Neutrophil granulocytes

Neutrophil granulocytes are the most common subtype of white blood cells (WBC) in peripheral blood and bone marrow. Their function is the first-line defense against microbes, inter alia represented in the fast recruitment by granulocyte colony-stimulating factor (G-CSF) in case of an inflammatory response, whereby the viability is only of short-term (several hours in blood). When rolling along the endothelium, the interaction between E-selectin (on endothelium) and sialyl-$Lewis^x$ (on neutrophil) is weak. However, in case of any inflammation with intracellular adhesion molecule 1 (ICAM-1) expression and interleukin 8 (IL-8 or CXCL8) secretion by endothelium, neutrophils are stimulated to walk through the endothelium (extravasation) (19).

Equipped with various effector molecules (in granules), such as toxic oxygen-derived products (H_2O_2), toxic nitrogen oxides (nitric oxide NO), antimicrobial peptides (defensins and cationic proteins), enzymes (lysozyme, myeloperoxidase)

and competitors (lactoferrin, vitamin B12-binding protein), neutrophils physiologically fight against bacteria and fungi. From a pathophysiological point of view, neutrophils play an important role during the initial phase of autoimmune diseases (e.g. multiple sclerosis, rheumatoid arthritis, atopic dermatitis) and allergies (19).

During granulopoiesis neutrophils arise from an oligopotent common myeloid progenitor (CMP) to become an oligopotent granulocyte/monocyte progenitor (GMP) and eventually differentiate into a granulocyte progenitor. Thereafter the maturation in the form of a sequential differentiation begins and the various steps can be found in the bone marrow smear as follows: myeloblast, promyelocyte, myelocyte, metamyelocyte, band neutrophil and, finally, segmented neutrophil (24). Granules appear for the first time throughout the transition from myeloblast into promyelocyte (primary granules). They likewise underlie a maturation process into secondary granules from myelocyte to metamyelocyte and into tertiary granules from band neutrophil to segmented neutrophil. Under physiological conditions mainly fully differentiated neutrophils leave bone marrow. However, when large numbers are needed due to high depletion during infection or cancer, the *emergency granulopoiesis* (25) mediated by G-CSF ensures that the granulopoiesis in the bone marrow is increased. There, many immature granulocytes leave the bone marrow and can be easily detected in differential blood counts.

1.3. Tumor immunology

To generalize the complexity of cancer, its biology can be characterized by eight *hallmarks (26)*, meaning the need for specific biological capabilities to assure the development and growth of the tumor and simultaneously have a comprehensive overview of its organization. These include *sustaining proliferative signaling, evading growth suppressors, resisting cell death, enabling replicative immortality, inducing angiogenesis, activating invasion and metastasis … reprogramming of energy metabolism and evading immune destruction* (26). Not only do these acquired abilities in conjunction with their complex functionality contribute to cancer biology and genome instability but also inflammation and the tumor

surroundings composed of putatively normal cells (including cells of the immune system) participate in fostering the outgrowth and helping to evade apoptosis of tumor cells (known as tumor microenvironment) (26).

A dichotomous role for immune cells in both antagonizing and enhancing tumor development is already known (26). There are many escape mechanisms used by tumor cells against the immune system. These include the secretion of immunosuppressive factors like transforming growth factor ß (TGFß) (27,28) or the recruitment of Tregs, which are intrinsically immunosuppressive, whereby both TGFß and Tregs suppress cytotoxic T cells (CTLs) and thus avoid detection or limit killing of cancer cells (29,30).

Interestingly, maintenance and enhancement of tumorigenesis by immune cells – largely by the innate immune system – is done by recruiting and abusing them in TME by secreted chemoattractants (26). Different mechanisms are already known, to give a few examples: the induction of angiogenesis, which is usually done by an *angiogenic switch* through countervailing factors such as vascular endothelial growth factor-A (VEGF-A), thrombospondin-1 (TSP-1) or fibroblast growth factor (FGF) (31,32), which can also be induced notably by cells of the innate immune system (33-36) .The facilitation of local invasion, usually performed by downregulation of attachment proteins within the cell sheet such as E-cadherin (37,38), can also be fostered by supplying matrix-degrading enzymes such as cysteine cathepsin proteases or metalloproteases from immune cells (39-42). Furthermore, by releasing chemicals, especially reactive oxygen species from macrophages, which are actively mutagenic for nearby cancer cells and are in favor of the acceleration of the malignant genetic evolution. Eventually, through inflammation itself by virtue of supplying bioactive molecules, which are then used as catalysts for tumor development (43-45).

Based on this, immune cells in the TME can be overruled and derailed from their actual functions. However, the absence of certain immune cells with the ensuing loss of immune surveillance, e.g. due to deficiencies in T lymphocytes and NK cells as observed in immunocompromised individuals, has adverse effects for preventing tumorigenesis (46,47).

Summarizing the observations above, it is clear that the complexity of tumor immunology is still not fully understood and delivers mainly double-edged results. The dichotomous role of immune cells in the TME is represented by the different tasks of the adaptive immunity (detecting and targeting antigens) and the innate immunity (clearing dead cells and fostering wound healing) (26) – fitting with the portrayal of tumors as *a wound that never heals* (48).

1.3.1. The role of neutrophils in cancer

Generally, myeloid cells are characterized by their high dynamic and adaptability. They are capable of taking on different functions simultaneously, which is mirrored in their functions in cancer with both pro- and anti-tumor effects (49). In the past, the role of neutrophils in cancer has been overshadowed by macrophages. Nevertheless, there are several clues that neutrophils actually play a bigger role in association with tumors and can primarily influence the behavior of other tumor-associated immune cells. This is mainly facilitated by aberrant cytokine production, which leads to adverse alterations of neutrophils addressing the tumor suppression. Moreover, complex interactions between several cytokines determine the effect on the target cell. The composition of these varies within the tumor type, its mutations and oxygen levels (50). Similar to physiological control loops, a pathological cytokine-loop representing an IL-17-G-CSF axis has been discovered consistent with systemic inflammation caused by tumor cells (50-57). Started with the secretion of IL-1ß by tumor cells, stromal cells or tumor-associated macrophages as a state of systemic inflammation, the secretion of IL-17 by γδ-T cells follows (50,58,59). This enhances the systemic G-CSF levels and consequently stimulates neutrophil expansion by releasing neutrophils from the bone marrow with an ensuing increased number of circulating neutrophils (50). It is assumed that with G-CSF as a pro-survival signaling also the lifespan of neutrophils is prolonged with an extended half-life of up to 17 hours not only locally – in vicinity to TME – but also systemically (50,60-63).

A subset of neutrophils has been shown to have immunosuppressive properties (50,59,64) due to their immaturity which has different functions, presumably by their different endowment of granules from those of mature neutrophils (50,59,65). Those immature neutrophils accomplish their function in inhibiting antitumor $CD8^+$ T cells whereby cancer cells successfully evade immune detection (59). Mouse

experiments have shown that intratumoral neutrophils, termed as *tumor-associated neutrophils* (TANs), after TGFβ-blockade acquired an antitumorigenic phenotype (N1), which decreased tumor growth by enhancing $CD8^+$ T cell activation opposed to TANs under TGFβ-exposure, which polarized into neutrophils with protumor properties (N2) (66,67). The exact mechanism of TANs in cancer is still unknown (68). However, TANs are suggested as important players in redirecting immune responses depending on TME (50,66). Moreover, there is still a need to shed light onto the question of a possible kinship between neutrophils and myeloid-derived suppressor cells (MDSCs) whether these are analogous or separate populations, because both share a common set of markers ($CD11b+Gr1^{high}$ in granulocytic or polymorphonuclear (G/PMN) opposed to $CD11b+Gr1^{low}$ in MDSCs). Due to their identical morphology a complete distinction is impossible, although the appearance of MDSCs is known only due to a pathological condition maintained by an aberrant expression of cytokines and by the fact that MDSCs are rarely found in physiological conditions. Therefore, both cell types (G/PMN-MDSCs) are referred to as *neutrophils with immunosuppressive capabilities* (50) with the ability to inhibit T cell proliferation, cytokine secretion and cytotoxic activity *in vitro* (69).

Additionally, neutrophils are versatile in promoting tumor initiation and tumor progression and likewise in limiting tumorigenesis. By producing reactive oxygen species (ROS) or reactive nitrogen species (RNS) and proteases, they contribute to epithelial damage, which empties into inflammation (50,70). Furthermore, the expression of inducible nitric oxide synthase (iNOS), arginase 1 (ARG1), fatty acid transport protein 2 (FATP2) for the release of prostaglandin E2 (PGE2) (69), and the signaling of TGFß lead to TAN-mediated T cell suppression (71,72). Neutrophils are further equipped with several mitogenic and pro-angiogenic molecules like neutrophil elastase (NE), prokineticin 2 (PROK2, also known as BV8) and matrix metalloproteinase 9 (MMP9) and therefore represent not only potent effectors of angiogenesis (50,73-79) but also facilitate the expedited seeding of metastasis by providing more routes for cancer cells to allow them to escape from the primary tumor (50). However, metastatic formation can also be limited by neutrophils through the expression of TSP-1, which is induced by a tumor-secreted peptide derived from prosaposin. TSP-1 can also be found on

primarily pro-metastatic $CD11b^{+}Gr1^{+}$ myeloid cells (50,80) and is in a steady interaction with tumor-derived opponent factors such as VEGF-A, TNFα, and TGFß (81,82) as an expression of the bidirectional but also contradictory interplay between TANs and cells of TME.

1.3.2. Neutrophils as therapeutic targets in ICI therapy

Neutrophil-targeting agents (such as Reparixin, CXCR1/2-antagonist) (83) would not only be interesting in cancer therapy but also be beneficial for treating several inflammatory and autoimmune diseases. The hitherto-contradictory role of neutrophils in anticancer therapy due to differences in tumor type, immune status of the host and mechanism of tumor killing chemotherapeutics leads to unresolved issues concerning the clinical benefit, notably reflected by the statement of a study in which neutrophils are even beneficial in early-stage lung cancer (50,84).

Currently no implementation of therapy strategies against neutrophils in NSCLC has been taken into account, but clinical trials are ongoing, predominately in the U.S., and are inhibiting specifically neutrophilic enzymes or their target proteins, such as:

- targeting the NOS:
  Phase Ib of L-NMMA and Pembrolizumab; Identifier: NCT03236935 (69,85).
- targeting the ARG1:
  Arginase Inhibitor INCB001158 as a Single Agent and in Combination With Immune Checkpoint Therapy in Patients With Advanced/Metastatic Solid Tumors; Identifier: NCT02903914 (69,86).
- targeting the PGE2-receptor:
  Grapiprant (ARY-007) and Pembrolizumab in Patients With Advanced or Metastatic Post-PD-1/L1 NSCLC Adenocarcinoma; Identifier: NCT03696212 (69,87).

Therapeutic synergies like anti-VEGF-A in combination with depletion of neutrophils by anti-Gr1 or anti-G-CSF antibodies could be amenable (88,89). The combination of T cell immune checkpoint inhibition together with neutrophil manipulation could also be a promising therapeutic approach (90). However, chemotherapeutics intrinsically induce neutropenia, which is apparently associated with improved survival in patients with NSCLC (91-94) which can also be

explained by the fact that neutropenia serves as a surrogate marker for the success of chemotherapy (50). Nevertheless, a deteriorating number of absolute neutrophils (ANC < 1,000/µL blood) goes hand in hand with a heightened risk of hazardous and life-threatening infections for the patient, so that a risk-benefit assessment always has to be performed before further therapy is initiated.

1.4. Cell analysis by flow cytometry

1.4.1. Principles of flow cytometry

Flow cytometry provides a vast range of possibilities to examine cells and their properties. In this regard, I do not claim to give complete explanations. For detailed information I refer to the producer's manuals and other kinds of literature for laboratory instruments.

Within the complexity of flow cytometry the most crucial facts are described below, especially those domains which played a significant role for the measurement of T cells.

In brief, a flow cytometer measures cells in suspension, which pass one by one through a measurement apparatus, using various wavelengths of light spectrum simultaneously to excite fluorescence in antibody-stained cells and detecting the emission light thereafter. Overall it is an interaction between moving cells through the system, optics for detecting cells, electronics for converting photons into electrons and data analysis software for a comprehensible depiction on a screen (95).

When a single cell passes through the laser beam, light of short wavelength scatters and thereby emits fluorescence. This phenomenon is nothing more than excited fluorescent molecules returning to unexcited ground-state by emitting light of longer wavelength. Eventually this lower energy in comparison to the excitation wavelength of high(er) energy is the information which is collected and then converted into electric signals (95).

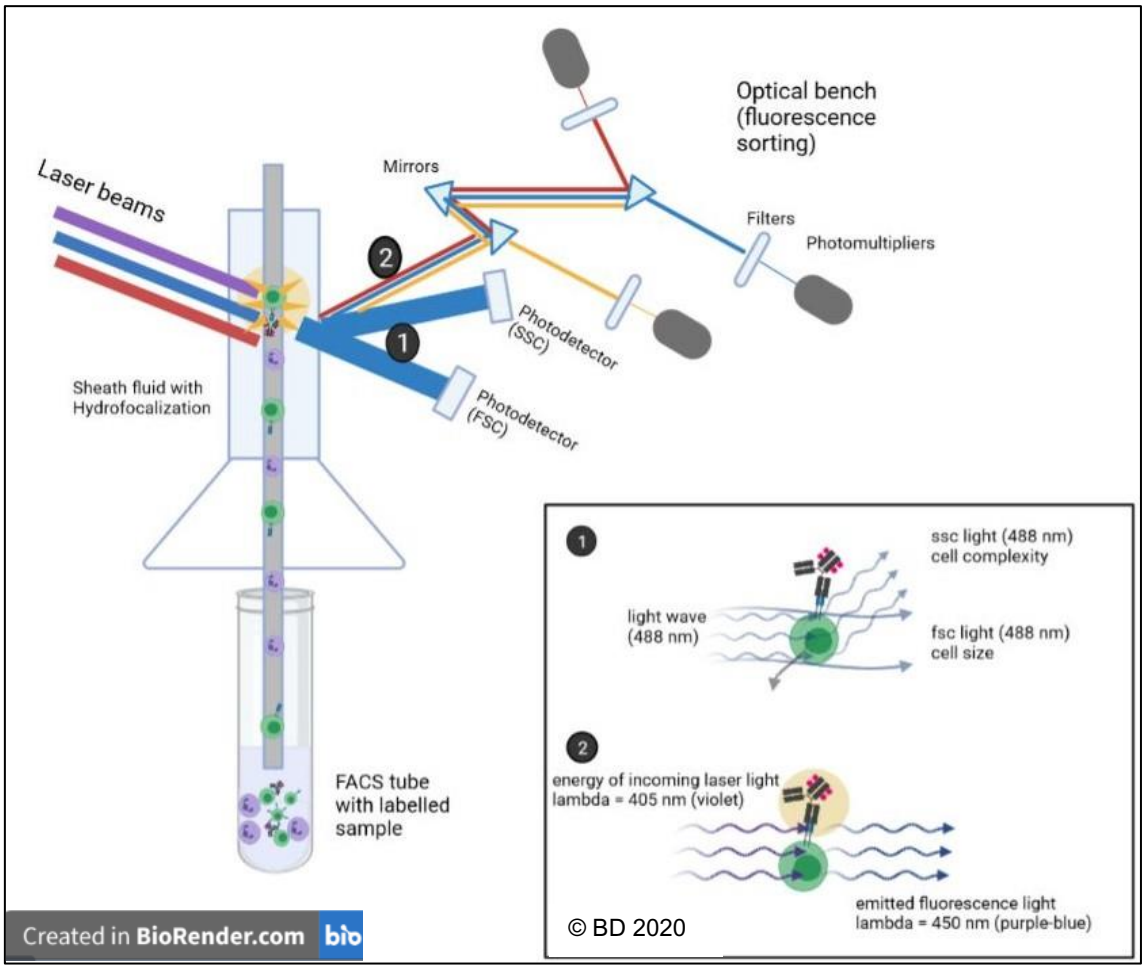

Figure 1: Principle of flow cytometry.

The sample with cell suspension is hydrodynamically focused by differential pressure between sample and sheath fluids and flows one by one in line (laminar flow) with sheath fluid through a laser, where the sample fluid flows in the center of the sheath and ordinarily does not mix with the sheath fluid. Reduction of the diameter within the cell flow leads to an acceleration and tapering of the sheath and the sample flow, called hydrodynamic (horizontal) focusing (95,96)*. When higher speed by means of heightened differential pressure is used and therefore the sample stream becomes wider, this results in less purity in single-cell analysis and thereby greater results of coincidence in data* (95)*.*
[1] When (even unstained) cells intersect a laser beam, they scatter light. They scatter either in line with illumination as the forward scatter (FSC), which is roughly proportional to cell size, or at 90 degrees to the illumination, called the side scatter (SSC) or right angle scatter, which represents the internal complexity/granularity of a cell (95)*. [2] With the excitation of a fluorophore on an antibody-stained cell by the corresponding laser beam, the fluorescent molecule first absorbs the energy from the incoming laser and then jumps back into a state of lower energy by emitting light of a longer wavelength than the laser beam ('Stoke's shift'), which is then going to be detected* (96)*.*

The optical system consists of a coherent, tightly defined, polarized and high-intensity light source (laser) with generally one single wavelength to stimulate the fluorescence, a filter system for separating the wavelengths and restricting a certain spectrum of emission (filter) and a measurement system, which captures and amplifies the emitted fluorescence (lens) by means of photodiodes for forward scatter and/or photomultiplier tubes (PMT) for side scatter and specific fluorescence (channel FL-1, FL-2, FL-3 until FL-8 for BD FACSCanto™ II). PMTs are very sensitive to weak signals; this sensitivity can be adjusted by changing the voltage, where the number of

electrons – proportional to arriving photons – is multiplied by heightening the voltage. In contrast, signals can be limited by a threshold where only signals with an intensity greater or equal to the threshold value will be processed and sent to the computer. If there is immunofluorescence, the signals are typically displayed as logarithmic scaling as a comprehensible depiction due to wide dynamic ranges found on cell surface markers. Hence, the signal runs through a detecting system, where it is first transduced from an optic signal into an electric signal and finally is turned into a digital signal (95,96)*. Figure was reproduced from Depince-Berger et al.: New tools in cytometry (97) and was also reproduced with permission of BD Biosciences (96).*

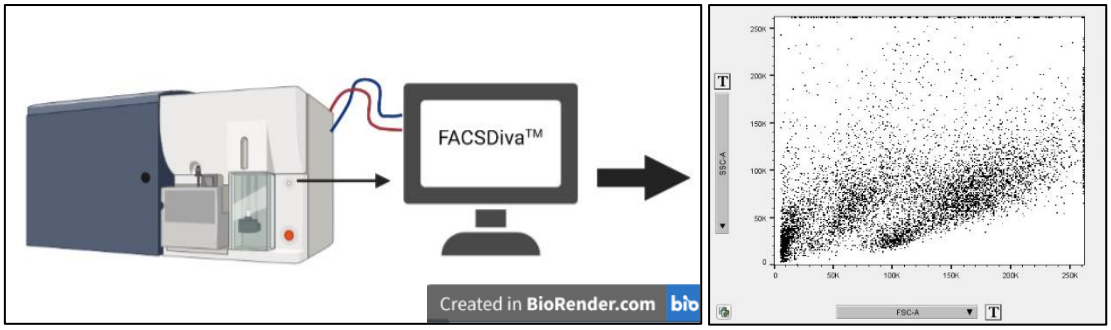

Figure 2: Acquisition of data.

Whenever fluorescence was detected by the flow cytometer, the signals were depicted in graphs by the data software. The default settings defined the x-axis as the brightness of fluorescence signal and the y-axis as the number of events in an univariate histogram – in this picture a bivariate dot plot with two parameters is depicted.

1.4.2. Immune cells on the screen

When flow data are acquired, there are many possibilities in depicting data to address properly the question.

Very generally, events can be displayed as an univariate plot (histogram) [A], where by default the x axis represents the intensity of the fluorescence and moves to the right when it is increasing; the y axis gives information about the number of events per channel. When events are portrayed as bivariate *plots* using dots [B], density [C] or contour plots [D], they allow to show data of two parameters and thereby identify more populations and also allow statistics of an area. Bivariate plots are the most common display format in flow cytometry (95,98).

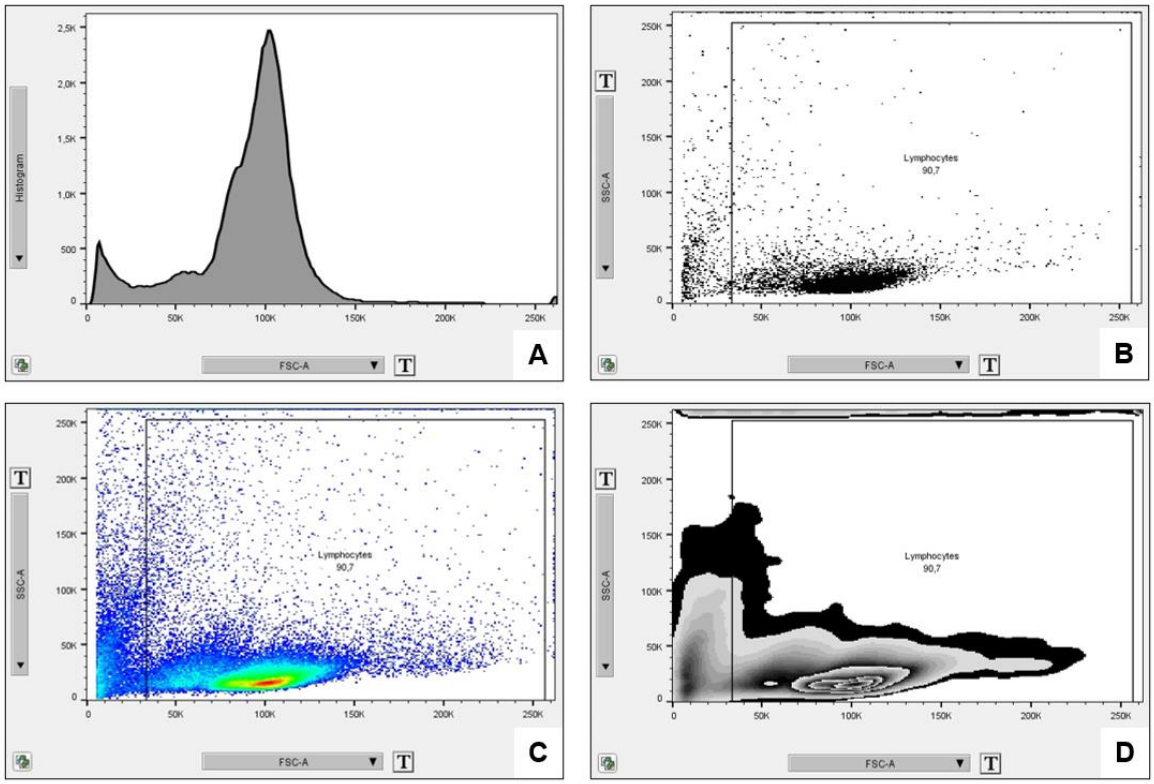

Figure 3: Depiction of anti-CD3 uncoated sample using univariate and bivariate plots.

Histograms [A] are beneficial in presenting normal distribution, identifying a specific subset or showing differences between populations using overlays. Only data of a single parameter can be shown by one dimension. In particular dot plots [B] depict the amount of data. By default the x axis shows the intensity of one parameter (fluorochrome or scatter) and moves to the right when increasing. The y axis represents the intensity of another parameter and moves to the top when increasing. A density plot or pseudo-color plot [C] uses color change to indicate an increasing density. When dots become too crowded together in a dot plot, density plots can be used to show where the concentrations are heaviest. The contour plot [D] has the option of being combined with displaying outliers as well, since the contour plot intrinsically would not display rare events very well. In this figure, a zebra plot as a kind of contour plot is depicted. (95,98).

1.4.3. Identification of immune cell properties

By using flow gates ('*gating*'), events of interest can be collected and analyzed according to the question. Based on this, statistical analysis and comparisons to different populations are feasible (98). The frequently used gating methods are depicted in figures 4-6, however, they merely show a few of the many of possibilities.

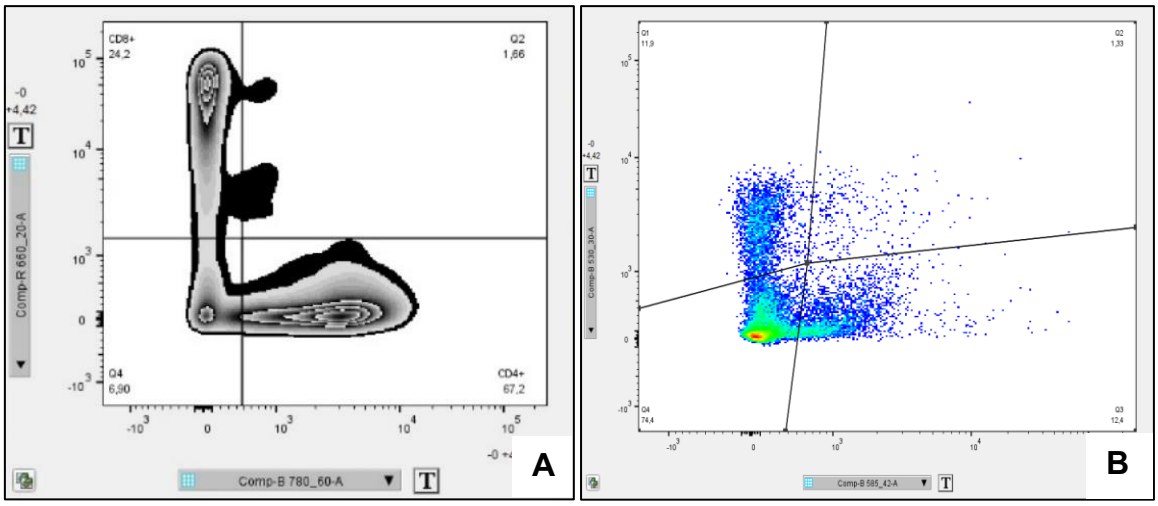

Figure 4: Quadrant and spider gate.

The quadrant gate [A] is useful for well resolved populations, where a set of two perpendicular lines divide the plot into four regions. The spider gate [B] is a variant of the quadrant gate, which allows to adjust the quadrants based on the distribution of data (95,98). Typically for FACS data, the numbers in the corner of each quadrant reflect the percentages of the respective region after gating.

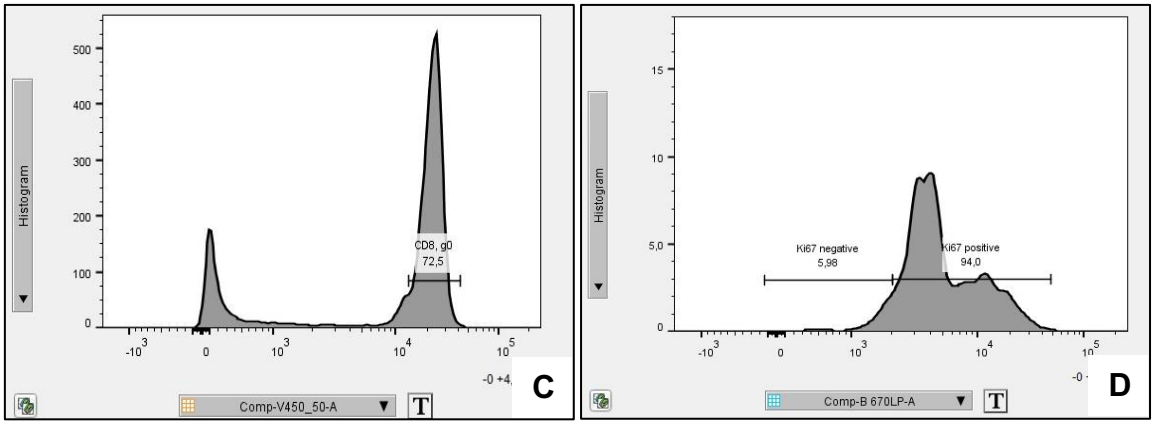

Figure 5: Range gate and bisector gate.

Range gates [C] and bisector gates [D] (95,98) *are used to analyze histograms. The number above the gate describes the percentage of the selected region, which is very useful for illustrating differences.*

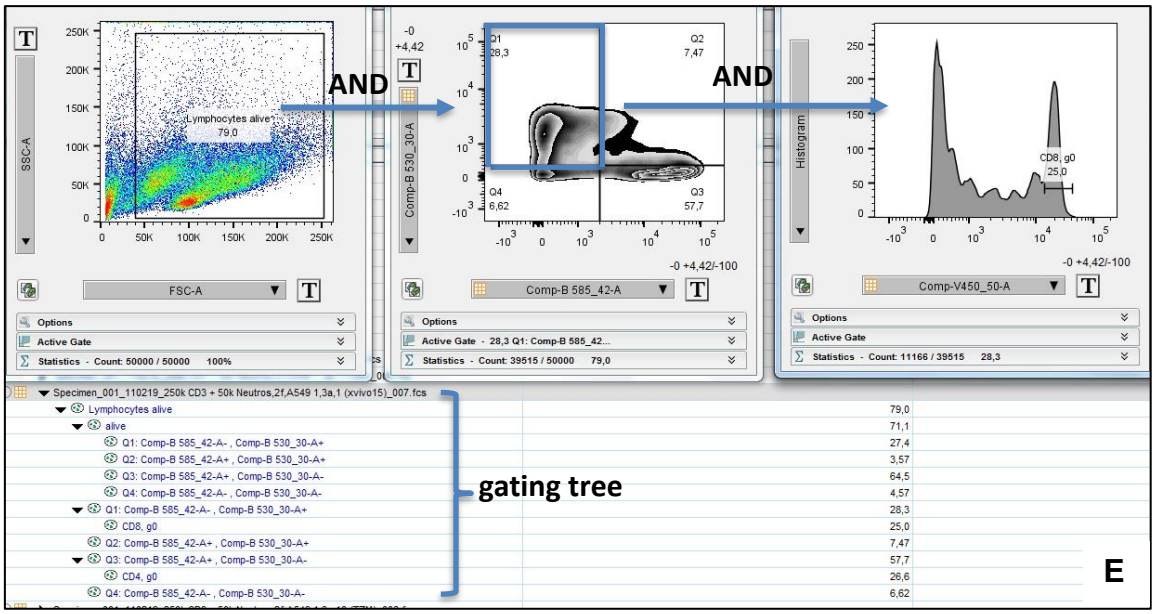

Figure 6: Boolean and hierarchical gating.

Experiments are mainly analyzed using complex ('Boolean') gating with its operating features such as AND/OR/NOT functions, where a defined population can be further analyzed for another property (95,98,99). *Equal to this, hierarchical gates [E] allows to organize the gating information as a "tree" with a parent gate and its descendants of children gates* (95,98).

2. Hypothesis

Studies have shown that TANs in the TME in NSCLC constitute the main immune cell fraction and have a strong negative correlation to T lymphocytes (18,100-105). Aim of this study was to complement existing data from mouse experiments, which have shown the promotion of tumor growth by inhibition of $CD8^+$ T cells through TANs (52,66,106-108). For that, I conducted co-culture experiments of human T cells together with neutrophils *in vitro* as part of an experimental setup. Co-cultures with naïve neutrophils and neutrophils, which were stimulated with supernatants of lung cancer cells or normal human bronchial epithelium to polarize them towards TANs, were compared to mono-cultured T cells. T cell proliferation and T cell apoptosis were analyzed using flow cytometry.

3. Materials and methods

This study was approved by the Ethics Committee of the Medical University of Graz and complies with the Declaration of Helsinki (EK-no.: 17-291 ex 05/06).

3.1. Blood collection

All blood samples stem from healthy donors with allergic or non-allergic history and were collected aseptically by venipuncture on the same day as they were used at the Otto Loewi Research Center, Division of Pharmacology, Medical University of Graz.

3.1.1. Extraction of cell factions

PBMC and PMNL were separated using sucrose density centrifugation (64) of 35 mL whole blood anticoagulated with 4.4 mL of **3,8% sodium-citrate** (tri-Natriumcitrat Dihydrat, 294.1 g/mol, Carl Roth®, #3580.1) at room temperature (RT).

After centrifuging 20 minutes at 300 g (RT) without brake, blood plasma (top layer) was carefully taken off and 6 mL of a **6% dextran solution** (360 mg/6mL 0.9% NaCl, Leuconostoc spp., Sigma-Aldrich, #31392) at RT were added to remove erythrocytes by sedimentation, then filled up to 50 mL with **physiological saline** ("Fresenius"-Infusionslösung 0.9%, Fresenius Kabi), carefully inverted two to three times and was left to settle for 30 min at RT to mesh erythrocytes together, whereupon they accumulate at the bottom of the tube.

The supernatant including the leukocytes was gently pipetted off and transferred to a new tube, which had been filled with **Histopaque®-1177** (Sigma-Aldrich; #10771) at RT and centrifuged at 300 g for 20 min (RT) without brake. Using Histopaque allows the separation of peripheral blood mononuclear cells (PBMCs) including lymphocytes and monocytes; and the higher density fraction of polymorphonuclear cells (PMNLs), represented by neutrophil and eosinophil granulocytes.

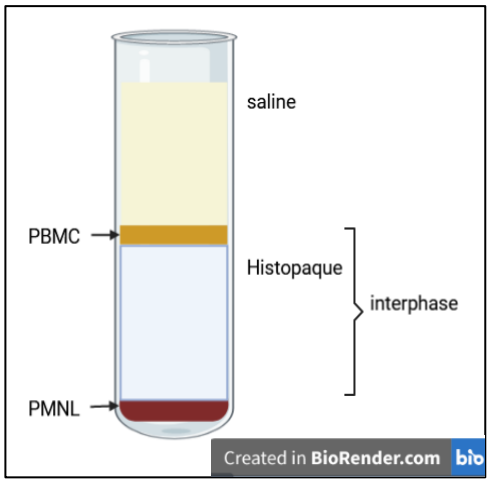

Figure 7: Fractioning of leukocytes using a density gradient.

The interphase, including PBMCs and Histopaque, and the PMNLs were the regions of interest. Practically the borders between the different phases were never completely distinct. Hence, it was crucial to pipette off the supernatant (saline) gently. PMNLs were still stuck with erythrocytes at the bottom of the tube, hence they appeared as a red fluid pellet.

For PBMC isolation, the saline phase was discarded (representing the top ~3 cm within the tube) using Pasteur pipettes. The interphase, consisting of PBMCs and a broader phase of Histopaque, was then aspirated out and transferred into a new tube. Histopaque was removed by filling up the tube to 50 mL with **HBSS** (Hanks' Balanced Salt Solution, Gibco™ HBSS without CaCl2/without MgCl2, Thermo Fisher Scientific, #14175053) and centrifuging 7 min at 300 g (RT) with brake. The supernatant was discarded and the leftover yellow solid pellet was resuspended in 10 mL HBSS for cell counting.

For PMNL isolation, the leftover red pellet was treated with a hypotonic shock lysis to remove the red blood cells (RBCs). For this, a washing step with 20 mL HBSS and centrifuging at 300 g for 7 min (RT) with brake occurred. Supernatant was carefully pipetted off and the pellet was resuspended properly in 1 mL of fresh by 0.2 µm syringe filter (VWR spp., #514-0061) sterile-filtered **0.2% saline** (100 mg NaCl/50 mL DI water) by pipetting up and down several times. The lysed pellet was filled to 10 mL with 0.2% saline and immediately supplemented with 10 mL sterile-filtered **1.6% saline** (800 mg NaCl/50 mL DI water) to reestablish physiological saline conditions. Finally, 10 mL HBSS were added to the cell suspension and spun 7 min at 300 g (RT) with brake. After this, supernatant was discarded and PMNL were resuspended in 10 mL HBSS for cell counting.

3.1.2. Isolation of T lymphocytes from PBMCs

T cells ($CD3^+$) were isolated using specific column-free magnets (EasySep™ Magnet, #18000, STEMCELL Technologies) including their magnetic kits (**EasySep™ Human T Cell Isolation Kit**, #17951, STEMCELL Technologies). In this procedure, monocytes and B lymphocytes were selectively enriched with

magnetic particles to stick these unwanted cells onto the tube surface by magnetism, whereby T lymphocytes stay in the buffer solution (negative selection method) (109). The vendor's instructions (109) were followed with the recommended work concentration of 5 x 10^7 PBMCs per mL. When the PBMC count deviated from the recommended work concentration, the volumes of the reagents were adjusted.

First, PBMCs were centrifuged gently at 300 g to 400 g for 5 min (RT). After this, the supernatant was discarded and cells were resuspended with 1 mL of the recommended *isolation buffer*, containing PBS(-/-) (phosphate-buffered saline without Calcium/Magnesium) with 2% FBS (fetal bovine serum) and 1 mM EDTA (109), and transferred into a 5 mL round-bottom tube. Then 50 µL of *Isolation Cocktail* (component# 17951C) was added to the sample, mixed and incubated for 5 min at RT. Meanwhile the *RapidSpheres* (component# 50103) vial was quickly vortexed for 30 seconds. After incubation, 40 µL of vortexed *RapidSpheres* was admixed to the sample and incubated for 5 min at RT once more. Finally, the sample was topped up to 2.5 mL with the recommended *isolation buffer* and mixed it all together by gently pipetting up and down, then the tube was placed without a lid into the magnet and waited for 5 min at RT. Finally, to yield the isolated T lymphocytes, the content of the magnet tube was discarded into a new empty tube with continuous movement.

3.1.3. Cell counting

For the experiments, it was essential to know about the exact cell count at any time. I commonly counted manually using the NEUBAUER counting chambers with **Kimura's staining solution** (110), generated by mixing several components through a pleated filter (type 595 ½) as follows:

- 11 mL 0.05% toluidine blue O (Sigma-Aldrich, #T3260)
- 5 mL of any phosphate buffer (pH 6,4)
- 0.8 mL 0.03% light green (Sigma-Aldrich, # L5382)
- 0.5 mL saturated saponin solution (Sigma-Aldrich, # 47036)

After putting 10 µL of cell suspension into 90 µL Kimura's blue (1:10 ratio), 10 µm of the stained cell suspension was pipetted into the counting chamber and a coverslip was put on. After that, cell counting was performed manually under the light microscope.

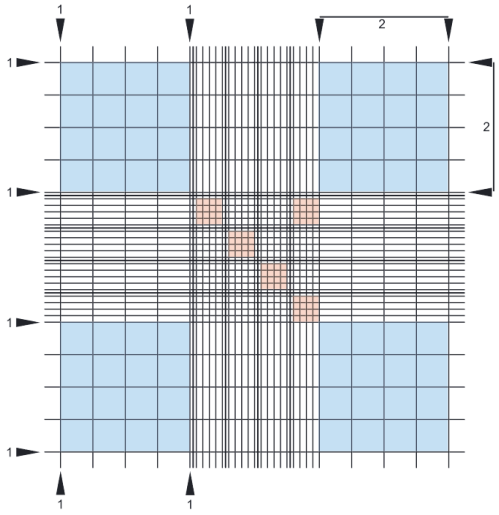

Figure 8: Microscopic view of the NEUBAUER counting chamber (112).

The counting grid is divided into nine large squares with an area of 1 mm^2 each, the depth of the chamber is 0.1 mm; the large corner squares are each divided into 16 little squares of 0.0025 mm^2 each (111). The counting of leukocytes merely occurs in the four large corner squares.

When cells touched the inner two of three border lines, they were counted in accordance with the border rule, where the middle line of the three border lines must be considered as the actual border. Rigorously, the mean cell count of the four squares is valid when the difference between the values of each square is lower than 10% (111). The following formula is proposed for calculation:

mean cell count of the four squares x 50 (as calculation factor in a 1:20 dilution) = cells/µL. (112)

I preferred a 1 to 10 dilution with a corresponding calculation factor of 100, computed up to 10 mL this is practically equivalent to a simplified formula as follows:

mean cell count of the four squares x 10^6 = cells/10 mL.

Only living cells were counted, whose membrane barriers were not demolished and thereby appeared as white or clear cells under the light microscope, otherwise they would have appeared as blue cells (dead cells).

3.1.4. Isolation of eosinophil granulocytes from PMNLs

For the following isolation of eosinophil granulocytes from PMNLs, the sample was prepared first by ascertaining the cell count in a NEUBAUER counting chamber, since the instructions for use of the isolation kit (**human Eosinophil Isolation Kit**, Miltenyi Biotec, #130-092-010) recommended each reagent volume described below for 1 x 10^7 total cells for the entire magnetic labeling procedure (113).

After counting, PMNLs were centrifuged for 10 min at 300 g (RT) with brake. Supernatant was then aspirated and cells were resuspended in 40 µL of *buffer*, composed of PBS(-/-) with 0.5% BSA (bovine serum albumin) and 2 mM EDTA (113). 10 µL of *human Eosinophil Biotin-Antibody-Cocktail* was properly admixed to the sample and incubated for 10 min in the refrigerator at 4 °C. After incubation, 30 µL of *buffer* were added and 20 µL of *Anti-Biotin MicroBeads* were admixed to the sample and left to settle for 15 min in the fridge at 4 °C. Finally, a washing step occurred by filling the sample up to 2 mL with *buffer* and centrifuging for 10 min at 300 g (RT) with brake. PMNLs were then resuspended in *buffer* at a concentration of 1 x 10^8 cells per 500 µL to proceed with the magnetic separation using magnetic columns (MACS® LS Column, Miltenyi Biotec, #130-042-401).

These were placed in an appropriate separator (e.g. MidiMACS™ Separator, Miltenyi Biotec , #130-042-302). By this, its magnetic field was amplified by 10,000-fold due to *superparamagnetic spheres* in the magnetic columns (114). Each column has a limited capacity of retaining approximately 1.5 x 10^8 cells – in this case capturing neutrophil granulocytes, whereas eosinophil granulocytes easily pass through (negative selection). The columns were initially saturated with 3 mL PBS(-/-), then the total cell suspension was pipetted incrementally onto it and the columns were rinsed again with 3 mL PBS(-/-) three times afterwards. The tube under the magnetic column picked up the dropping eosinophil granulocytes and was then spun 10 min at 300 g (RT) to remove its supernatant, whereby the neutrophil granulocytes still stuck in the columns.

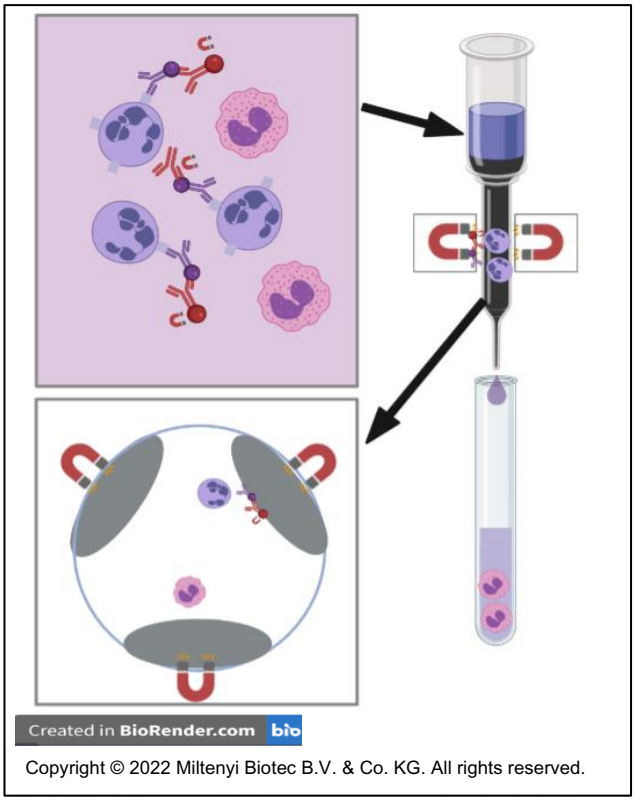

Figure 9: Magnetic isolation of eosinophils. When the cell suspension was trickled onto the column, the cells passed through a magnetic field. The labeled cells (neutrophils) were retained only by magnetic forces, in contrast to unlabeled cells (eosinophils) which could move between the 'cell-friendly coated superparamagnetic spheres' (114) inside the column due to negative selection – here a MACS® LD column is illustrated. The space between the spheres is 20 times bigger than the size of lymphocytes – here portrayed as a cross-section through a column. Figure was reproduced with permission of Miltenyi Biotec (113,114).

3.1.5. Isolation of neutrophil granulocytes from PMNLs

After the isolation of eosinophil granulocytes, the magnetically labeled neutrophils were still bound to magnetic beads and remained in the column. To retrieve the desired cells, the column was taken out of the magnetic field and cells were then carefully pressed out by a plunger.

After applying mechanical pressure on the neutrophils, the question, whether neutrophils had been activated and thereby had lost their cell integrity and capability of being activated by cytokines, was answered by performing a neutrophil *shape change assay* – a well-known method in the lab (115). For evaluating neutrophil activation, dose-response curves were examined and are further described in chapter 4.1..

3.1.6. Neutrophil shape change assay

Using an established shape change assay (115), the naïve neutrophils from untreated PMNLs were compared with isolated neutrophils after magnetic isolation (see details 3.1.4. and 3.1.5.). Thereby, changes in forward scatter (FSC) properties in response to the neutrophil activating cytokine IL-8 in serial dilutions were examined (chapter 4.1.). To measure the FSC, a BD FACSCanto™ II flow cytometer (BD Biosciences) was used.

For this, two rows of 10 tubes each were prepared. In each tube 50 µL PBS(+/+) or 50 µL PBS(+/+)-IL-8 solution was mixed together with 50 µL of cell suspension from either PMNLs or isolated neutrophils. To simplify the work steps, the first row was prepared with double the amounts of PBS(+/+) or PBS(+/+)-IL-8 solution before half of the volume from the first row was transferred into the second row. The highest examined end concentration of IL-8 after adding cell suspension was 10 nM and serial dilutions were made for nine conditions plus one negative control.

Finally, 50 µL cell suspension either from PMNLs or isolated neutrophils was added and all samples were gently agitated by vortexing. The panel incubated in a water bath for 4min at 37 °C. To stop neutrophil activation prior to analysis by flow cytometry, each tube received 150 µL of cold **fix solution** (BD CellFIX™ 10 X, BD Biosciences, #340181, diluted to 1 X in BD FACSFlow™ and Aqua dest.) and was incubating at 4 °C in the fridge in the dark while the instrument was prepared.

3.2. Tumor cell culture

For the pre-treatment of neutrophils to simulate tumor microenvironment conditions, supernatants from A549 and BEAS-2B cells were generated.

3.2.1. Cell lines and used ingredients

Cell lines from A549 and BEAS-2B (in the experiments signed with B2B) were cultured to extract their supernatants. The A549 cell line represented tumor cells from human lung adenocarcinoma, whereas the BEAS-2B cell line represented *immortal but non-tumorigenic cells (116)* derived from normal human bronchial epithelium (116-119).

Trypsin/EDTA (trypsin 0.05%/EDTA 0.02% in PBS, PAN-Biotech™, #P10-023100) was used as a proteolytic enzyme for cutting cell connections and **DPBS(-/-)** (Dulbecco's phosphate buffered saline) for the washing steps. **DMEM(++)** (Dulbecco's Modified Eagle's Medium with 10% FBS and 1% PS) or **DMEM(+-)** (without PS) was used as nutrient medium (each DMEM, high glucose, Gibco™, Thermo Fisher Scientific, #41965039).

3.2.2. Storage and freeze/thaw procedures

For long time storage cell lines are frozen in sterile-filtered freezing media (FBS with 10% DMSO) in liquid nitrogen.

Thawing: Freezing media contains DMSO (dimethyl sulfoxide) to prevent the formation of water crystals. Therefore, it was necessary to thaw cells quickly in a water bath or incubator and, once thawed, to free them immediately from the DMSO due to the cytotoxic effects of DMSO on cells at room temperature. Hence, the cells were immediately pipetted sterilely using filter tips in 10 mL of medium (DMEM) and were then centrifuged at 500 g for 5 min (at RT). Subsequently, and to work with higher cell concentrations, the cells were seeded in small flasks (T-75 cm²) with 5 mL to 6 mL of either DMEM(++) or DMEM(+-), the latter was used for mycoplasma testing.

Freezing: First, the medium from the remaining cells was removed by centrifuging 5 min at 1,500 g (RT) and discarding the supernatant. The cell pellet was then resuspended in freezing medium at a concentration of 3 x 10^6 cells/mL. After this, the cell suspension was aliquoted into cryovials (cryogenic storage vial, e.g. ThermoFisher Scientific, #5000-1020) with 1 mL per vial, consequently slowly cooled down to -1 degree per minute in a Mr. Frosty (Thermo Scientific™ Mr. Frosty, Thermo Fisher Scientific, #5100-0001) filled with 100% isopropyl alcohol. The cell suspensions were finally stored in liquid nitrogen.

3.2.3. Cell collection and splitting of cells

After cells had been thawed and had reached an estimated cell proportion of ~90% by volume (by eye under a light microscope), it was necessary to split them. I commonly started with two small flasks (T-75 cm²). The first flask with DMEM(++) and its cells was transferred into two empty big flasks (T-175 cm²), equal to a splitting ratio of ~1 to 8 when the volume of a T-75 cm² flask corresponds to a quarter of the volume of a T-175 cm² flask. The cells of the second small flask with DMEM(+-) were cultured for 48 hours in antibiotic-free medium to test for mycoplasma.

When 80-90% confluent, media from flasks with cells were removed to split cells into new flasks or to use for experiments. 5-10 mL of warm PBS(-/-) was then used in a washing step to remove any possible remaining traces from the media

(DMEM), containing FBS, which unfavorably neutralizes trypsin. 1-5 mL trypsin was used to detach cells and incubated for 5 min maximum in an incubator at 37 °C (RT also possible). A check under the light microscope revealed whether the cells were detached or needed a longer incubation time. When detached, 5-10 mL DMEM(++) was used to resuspend the cells into a single cell suspension by thoroughly pipetting up and down. This was done to avoid any adherence on the flask and any cluster formation, which can occur with adherent cells. A washing step by centrifuging 5 min at 1,500 g (RT) occurred to remove the trypsin entirely. The supernatants were carefully discarded and cells were resuspended in media.

3.2.4. Mycoplasma detection test

Cells were cultured on coverslips in 6-well plates in DMEM(+-) overnight. 6-well plates with coverslips were washed once with PBS(-/-) and fixed with 3 mL of ~4% PFA solution (paraformaldehyde, composed of 37% formaldehyde diluted in PBS(-/-) in 1:10 ratio) for 10 min (at RT). It was then washed again twice with PBS(-/-) and left to air dry. Subsequently, one drop of **DAPI** (= 4′,6-Diamidin-2-phenylindol, Vectashield® H-1200) was dropped on each coverslip and dried in the dark. Finally, it was checked under a fluorescence microscope for mycoplasma contamination.

3.2.5. Cell supernatants – seeding, starving and harvesting

For the cell count, an automated cell counter (e.g. NucleoCounter® NC-200™) was used. Based on the cell counting, 1 x 10^6 cells/well in 24-well plates were seeded for 24 hours. A check under the light microscope followed. After this, the medium was changed by gently discarding all DMEM(++) and replacing with 500 µL of DMEM(--) for the next 24 hours to induce starvation of the cells to simulate the undersupply in rapid growing cells. The next day, 450 µL of cell supernatant from each well was pooled into a 15 mL Falcon tube and centrifuged 5 min at 1,500 g (RT) to filter out possible unwanted cells. Following this, 1mL of supernatant was transferred into Eppendorf tubes and immediately frozen in liquid nitrogen for the ensuing storage at -80 °C.

3.3. T cell proliferation assay

3.3.1. T cell mono-culture

T cell medium: For assessing (a possible inhibition of) T cell proliferation among different conditions, especially in the presence of neutrophils, beneficial growing conditions for T cells had to be ensured first. This included the preparation of isolated T cells with a corresponding proper T cell medium with included growth factors and buffers, which ensured the outgrowth of T cells within three and six days. Therefore, an established T cell medium recipe (120,121) was used as described in table 1, or with XVivo15 (TheraPEAK™ X-VIVO™-15 Serum-free Hematopoietic Cell Medium, Lonza, #BEBP02-061Q) instead of RPMI and FBS in the medium.

Table 1: Recipe for T cell medium for 5 mL.

amount (stock concentration)	**substance**	**end concentration** (in T cell medium)
4,263.75 µL	RPMI-1640 cell culture medium	base liquid
500 µL (100 Vol.%)	FBS	10 Vol.%
125 µL (1 M)	HEPES	25 mM
50 µL (100 Vol.%)	PS	1 Vol.%
50 µL (200 mM)	L-Glutamine	2 mM
5 µL (50 mM)	beta-Mercaptoethanol	50 µM
5 µL (1 mg/mL)	anti-human CD28.2	1 µg/mL
1.25 µL (20 µg/mL)	human IL-2	5 ng/mL
in total 5,000 µL		

*Material list (enumerated): **RPMI** 1640 Medium, Gibco™, Thermo Fisher Scientific, #21875034; **FBS** (FBS GAMMA IRRAD S.AMERICAN(CE)), Thermo Fisher Scientific, #10499044; **HEPES**, Gibco™, Thermo Fisher Scientific, #15630080; **Penicillin-Streptomycin**, 10,000 U/ml Penicillin, 10 mg/ml Streptomycin, PAN-Biotech™, #P06-07100; **L-Glutamine**, Gibco™, Fisher Scientific, #25030081; **beta-Mercaptoethanol**, Gibco™, Thermo Fisher Scientific, # 31350010; Ultra-LEAF™ Purified **anti-human CD28 Antibody**, BioLegend®, #302934; **human IL-2** Recombinant Protein, Gibco™, Thermo Fisher Scientific, #PHC0026*

T cell isolation: As described in chapter 3.1.2., T lymphocytes from PBMCs were isolated using magnetic kits. For ascertaining the proper count of T cells and subsequent concentration in the medium, the NEUBAUER counting chamber (chapter 2.1.3.) was used. Due to the abundancy of successfully isolated $CD3^+$ T cells, the T cell proliferation assay could be conducted with a work concentration of 2.5 x 10^5 cells per 100 µL.

CD3 antigen coating: For seeding T cells, a 96-well plate with round bottom (Greiner-CELLSTAR®-96-Well-Platten, Greiner Bio-One, #650180) was used. Additionally, each well had been coated with **human anti-CD3** (Ultra-LEAF™ Purified anti-human CD3 Antibody, BioLegend®, #317326, stock concentration 1 mg/mL) to activate the T cell receptor which leads to T cell activation and proliferation.

Therefore, anti-CD3 was diluted in PBS(-/-) in 1:200 ratio at a concentration of 5 µg/mL. Each well was then filled up with 200 µL of diluted anti-CD3 solution. The plate was sealed with parafilm (paraffin wax) to protect against evaporation and was stored cooled in the fridge at 4 °C overnight. The CD3-coating was completed the next day before seeding. The 200 µL anti-CD3 solution was sucked off with autoclaved glass tips and washed with 200 µL PBS(-/-) and repeated for overall three times in the sterile workbench.

Incubation: When T cells were seeded, the set wells thrived in an incubator at 37 °C for three and six days. T cell medium was changed after 48 to 72 hours when the medium color of RPMI turned yellow (unfortunately not visible in XVivo15) due to waste cell products or disrupted homeostasis, in particular acidosis by cell metabolism and due to used up nutrients. For this, 5 mL of T cell medium was newly prepared, then 100 µL fluid of each well was carefully pipetted off (as T cells are non-adherent on wells) and filled up with fresh medium without mixing.

Cells were harvested after in mean three (± 1) and six (± 1) days and were transferred into FACS tubes (BD Falcon™ tubes 12 x 75-mm) for the respective condition to create a panel for the ensuing staining.

Work steps regarding the seeding of cells or the handling with T cell medium were performed sterilely on a sterile work bench. This especially refers to the CD3-

antigen coating, the mixture of T cell medium and the seeding of cells into the wells. All other work steps were performed under standard laboratory conditions.

3.3.2. T cell and neutrophil co-culture

Additional to T cell mono-culture, neutrophils were treated with supernatants, before they were seeded with T cells.

Treatment of neutrophils: After retrieving neutrophils from PMNLs (chapter 3.1.5.), (tumor) cell supernatants from A549 and BEAS-2B (chapter 3.2.1.), which were stored at -80 °C, were prepared by thawing them slowly on ice.

Five overall conditions in Eppendorf tubes were set up, whereby the volume of cell supernatant (in µL) was either equal to the volume of cell suspension (1:1) or proportional to a twentieth of cell suspension (1:20), or where no treatment was carried out (naïve). The idea was that the (tumor) cell cytokines within the supernatants should alter the integrity of neutrophils. RPMI or XVivo15 media were used for the dilution of the supernatants or for media alone controls. For this, the neutrophil suspension was prepared in a work concentration of 2 x 10^5 cells per 100 µL of medium before mixing with supernatants. Neutrophils were counted using an automated cell counter (such as EVE^{TM}, NanoEntek), which also ascertained the percentage of viability of neutrophils (mostly over 85%). Then, the neutrophils were merged with the respective supernatant and incubated for 1 hour at RT.

After incubation, the treated cells were centrifuged 7 min at 400 g (RT). The supernatants were then removed by gentle pipetting off without losing any cells from the pellet. Finally, neutrophils were resuspended in T cell medium into a concentration of 5 x 10^4 cells per 50 µL.

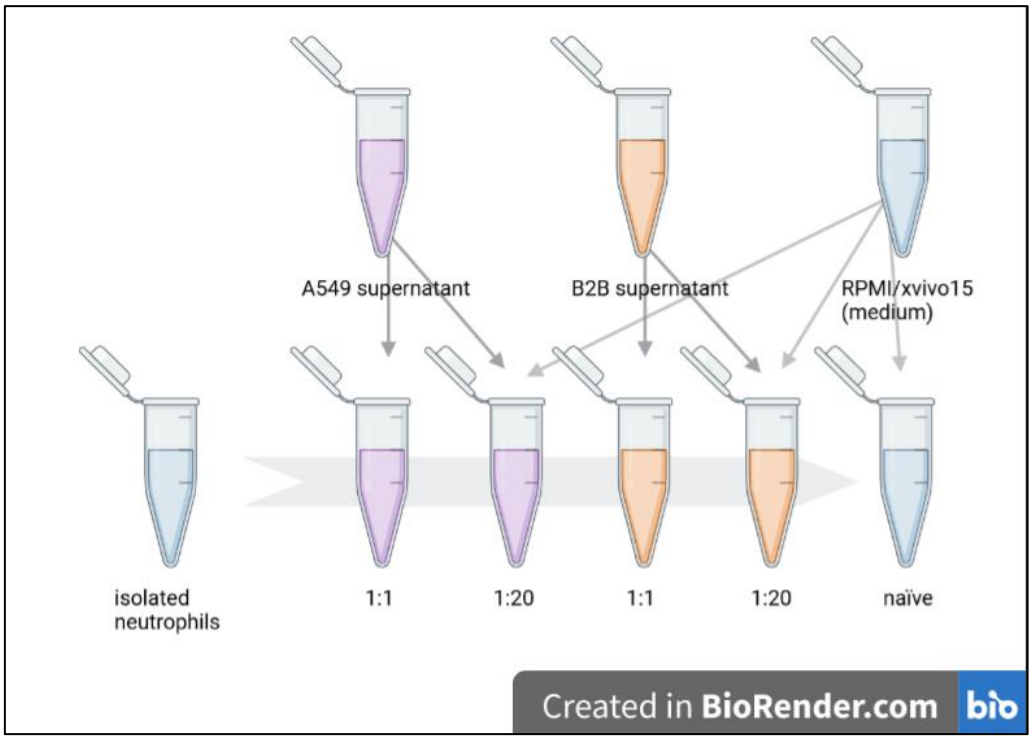

Figure 10: Treatment of neutrophils.

Five overall conditions in Eppendorf tubes were set up with the respective supernatant in two different concentrations (in 1:1 or 1:20 ratio) and one for naïve neutrophils as control. The exact number of used reagents are described in table 2.

Table 2: Treatment of neutrophils.

sample	**cell suspension**	**supernatant**
A549 (1:1)	each with 2 x 10^5 neutrophils resuspended in 100 µL of medium*	**+** 100 µL A549 supernatant
A549 (1:20)		**+** 10 µL A549 supernatant + **+** 90 µL medium*
B2B (1:1)		**+** 100 µL B2B supernatant
B2B (1:20)		**+** 10 µL B2B supernatant + **+** 90 µL medium*
naïve neutrophils	2 x 10^5 neutrophils (untreated) resuspended in 200 µL of medium*	**-**

**After incubation of 1 hour, the cells were immediately centrifuged and resuspended in T cell medium (*containing RPMI, or XVivo15 in later course).*

Seeding T cells and neutrophils: After isolation from PBMCs, 2.5 x 10^5 T cells resuspended in 100 µL-prewarmed T cell medium were filled into each well of the coated 96-well plate (figure 11). After this, 5 x 10^4 treated neutrophils resuspended in 50 µL T cell medium were merged to the corresponding wells. Finally, additional 50 µL of T cell medium was added to all wells to reach a total of 200 µL/well.

Some wells were used for T cell mono-cultures with 2.5 x 10^5 T cells per 100 µL and served as negative control and were also used as single-color control for the flow cytometer setup (chapter 3.5.). These wells have received additional 100 µL of T cell medium to match with the conditions of co-culturing.

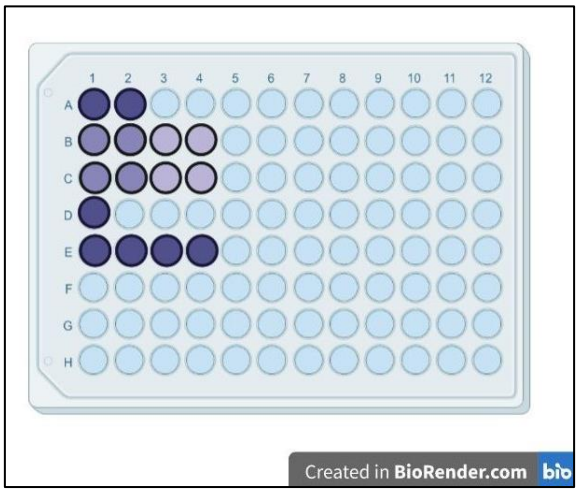

(A1) 2.5 x 10^5 T cells with 5 x 10^4 neutrophils (naïve), 3 days
(A2) 2.5 x 10^5 T cells with 5 x 10^4 neutrophils (naïve), 6 days
(B1) 2.5 x 10^5 T cells with 5 x 10^4 neutrophils (A549 1:1), 3 days
(B2) 2.5 x 10^5 T cells with 5 x 10^4 neutrophils (A549 1:20), 3 days
(B3) 2.5 x 10^5 T cells with 5 x 10^4 neutrophils (B2B 1:1), 3 days
(B4) 2.5 x 10^5 T cells with 5 x 10^4 neutrophils (B2B 1:20), 3 days
(C1) 2.5 x 10^5 T cells with 5 x 10^4 neutrophils (A549 1:1), 6 days
(C2) 2.5 x 10^5 T cells with 5 x 10^4 neutrophils (A549 1:20), 6 days
(C3) 2.5 x 10^5 T cells with 5 x 10^4 neutrophils (B2B 1:1), 6 days
(C4) 2.5 x 10^5 T cells with 5 x 10^4 neutrophils (B2B 1:20), 6 days
(D1) 2.5 x 10^5 T cells (mono-culture)
(E1) 2.5 x 10^5 T cells (single-color, $CD4^+$ dye)
(E2) 2.5 x 10^5 T cells (single-color, $CD8^+$ dye)
(E3) 2.5 x 10^5 T cells (single-color, proliferation dye)
(E4) 2.5 x 10^5 T cells (unstained)

Figure 11: Example of conditions in co-culturing of T cells and neutrophils.

These conditions represent the repeatedly performed co-culturing for the T cell proliferation assay for three and six days. I always set up more wells for the ensuing single-color staining for FACS compensation (E1 – E3) and one unstained sample for detecting autofluorescence (E4).

3.3.3. T cell staining for flow cytometric analysis

T cells were stained for CD4 and CD8 by surface antigen staining to separate T cell subsets and with eF450 proliferation dye to ascertain proliferation behavior for each subset. Each condition (A1 to D1 in figure 11) was stained as multicolor sample, whereas the additional wells for single-color received their respective dye only.

Proliferation dye: Before seeded, the isolated $CD3^+$ T cells were labeled with the proliferation dye **eF450** (eBioscience™ Cell Proliferation Dye Fluor™ 450, ThermoFisher Scientific, #65-0842-85, stock concentration of 10 mM), details in chapter 3.5.3.1..

Surface antigen staining: When harvested, T cells were stained for CD4 and CD8 (table 3) in accordance with the surface antigen staining protocol (chapter 3.5.3.2.). The selection of the fluorochromes was limited by the combinations of dyes (chapter 3.5.2.).

Table 3: Multicolor sample for surface antigen staining in T cell proliferation assay.

reagent	stock [c]	volume/test	end [c]
CD4-PE	0.1 mg/mL	0.5 µL	0.25 ng/100 µL
CD8-FITC	0.5 mg/mL	1 µL	5 ng/100 µL
SB		48.5 µL	

The staining with eF450 had been done before and is part of the cell preparation throughout co-culturing. PE = phycoerythrin, FITC =fluorescein , SB = staining buffer.

*Material list: **CD4-PE** (Phycoerythrin anti-human CD4 Antibody), BioLegend®, #300508, clone: RPA-T4, stock concentration 0.1 mg/mL; **CD8-FITC** (Fluorescein anti-human CD8a Antibody), BioLegend®, #301006, clone: RPA-T8, stock concentration 0.5 mg/mL*

T cell proliferation for each condition was then measured by a BD FACSCanto™ II flow cytometer (BD Biosciences).

3.4. T cell apoptosis assay

T cell apoptosis was measured using PI/Annexin V apoptosis dye. In brief, cells were co-cultured as described above for 24 and 48 hours and subsequently stained.

In difference to the aforementioned T cell proliferation assay, T cell medium was altered by halving FBS to an end concentration in medium of 5 Vol.% (also replaced with XVivo15 thereafter), and proliferation dye had been omitted. However, after harvest, T cells were stained for CD4 and CD8, and subsequently stained with PI and Annexin V (chapter 3.5.3.2.). Multicolor and single-color samples for surface antigen staining were adapted to apoptosis dye and consequently led to different fluorochromes.

Table 4: Multicolor sample for surface antigen staining in T cell apoptosis assay.

reagent	stock [c]	volume/test	end [c]
CD4-PE-Cy7	0.2 mg/mL	5 µL	50 ng/100 µL
CD8-APC	0.05 mg/mL	5 µL	12.5 ng/100 µL
SB		40 µL	

The apoptosis dye followed thereafter in accordance with the supplier's instructions for use (122). Cy7 = cyanine7, APC = allophycocyanin, SB = staining buffer.

*Material list: **CD4-PE-Cy7** (PE/Cyanine7 anti-human CD4 Antibody), BioLegend®, #300512, clone: RPA-T4, stock concentration 0.2 mg/mL; **CD8-APC** (APC anti-human CD8a Antibody), BioLegend®, #301014, clone: RPA-T8, stock concentration 50 µg/mL*

3.5. Immunostaining for flow cytometry

3.5.1. Selection of antibody dyes

There is a large selection of purchasable antibody dyes and combinations of them.

In the panels, only monoclonal antibodies were used by virtue of their high specificity and low cross-reactivity. Furthermore, direct (without second antibody) antibody dyes were used, where antibodies had been already attached to fluorochromes, and purchased from vendors specialized in generating biological material for laboratory experiments (95).

In most cases suppliers gave enough information about their individual fluorophores (table 5 in chapter 4.2.) – especially the stain index (SI) was used to decide on a fluorophore for the panels. The higher the stain index the better the distinction in contrast to background/negative signals, i.e. high resolution and sensitivity even on surfaces with (expected) low-density antigens (95).

The selection of dyes was limited by the laser equipment from the used flow cytometer (BD FACSCanto™ II) in the lab. Hence, by its given three lasers of red (633 nm), blue (488 nm) and violet (405 nm) light and attached filters (123), it was feasible to extrapolate the amenable fluorophores (table 5 in chapter 4.2.).

3.5.2. Limitations of combinations

With multicolor experiments, combinations of various fluorochromes are limited owing to their exciting and emission spectra. Additionally, the combination also depends on the amount of antigen expression on the cell surface, where a highly expressed antigen should be tagged with a less bright fluorochrome and vice versa (95,99). The more colors are used, the more problems will emerge by the loss of resolution of dim signals (95).

With a spectra viewer from suppliers (in this case from the website of ThermoFisher Scientific) it was possible to check the intended multicolor panel together with the corresponding laser equipment from the used flow cytometer for any emission spillover (figures 22 and 26). This was used as an initial assessment for further compensation as well.

3.5.3. Staining protocol

For the question on surface antigens (CD4 and CD8) I primarily applied the in-house established surface antibody staining protocol (first stain, then fix) (64,120,121,124). As part of the dynamic optimizing process, the established staining protocol had been advanced with apoptosis dye.

In both the T cell proliferation assay and the T cell apoptosis assay, the protocol for surface antigen staining was implemented.

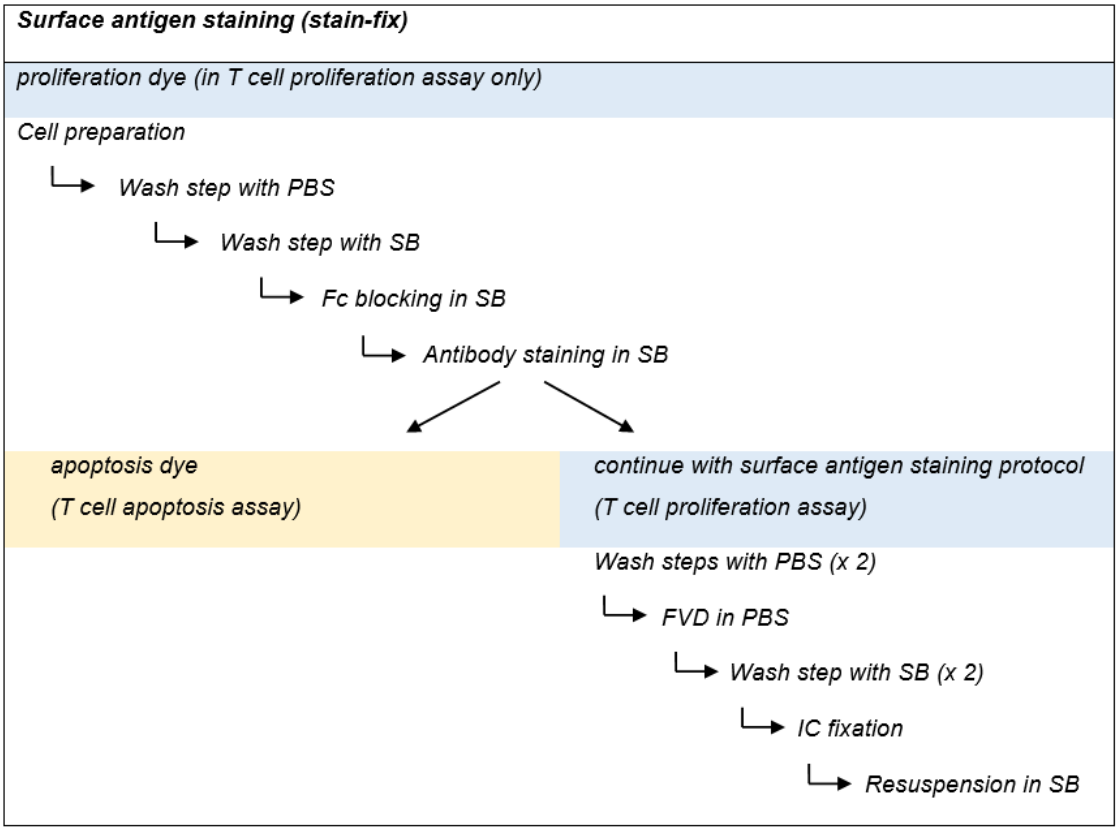

Figure 12: Algorithm of the in-house established surface antibody staining protocol.

Both the T cell proliferation assay and the T cell apoptosis assay required the surface antigen staining protocol to detect the T cell subsets ($CD4^+$ and $CD8^+$). PBS = phosphate-buffered saline, SB = staining buffer, FVD = fixable viability dye.

3.5.3.1. Used dyes before sowing

Proliferation dye: In T cell proliferation assay, T cells were prepared as 1 x 10^7 cells per mL. The equal volume (in mL) of eF450 dissolved in warm PBS(-/-) had been prepared with twice the work concentration of 10 µM and was then admixed directly to the cell suspension to an end concentration of 5 µM.

T cells incubated for 10 min at 37 °C in the dark (in a water bath or incubator) to prevent bleaching. After this, the stained T cells were washed with a 4-fold volume of staining buffer (PBS(-/-) with 2% FBS) and were left to settle for 1 min at RT in the dark. Finally, T cells were spun 7 min at 400 g (RT) and were resuspended in T cell medium after removing their supernatant.

During each mitosis cycle, the eF450 staining halves within the T cell and the fluorescence signal become less with each new generation (figure 13) (125).

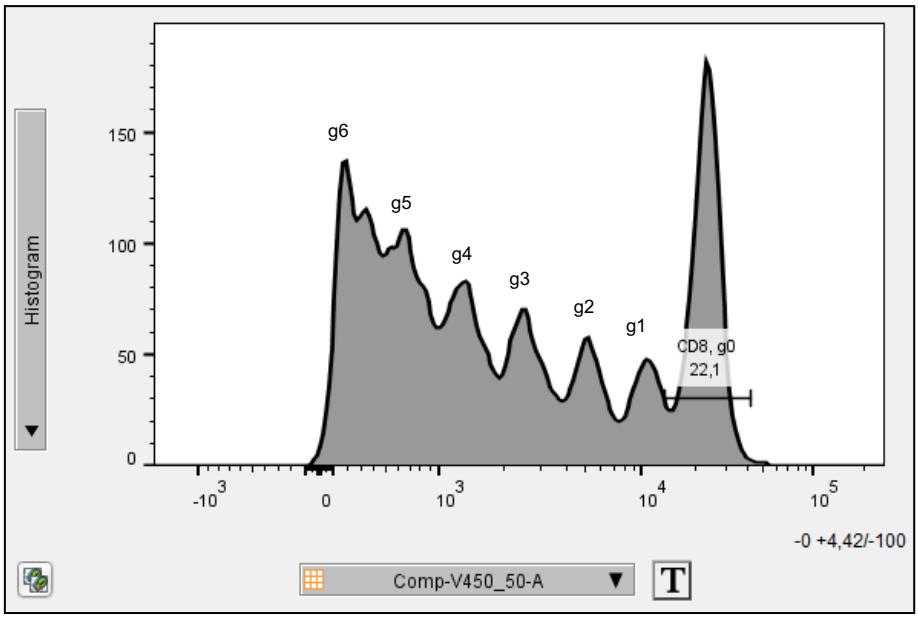

Figure 13: Proliferation of T cells detected by eF450 proliferation dye.

With each mitosis the signal of eF450 halves within the T cell as can be seen in a reduction of the fluorescence signal per mitosis simultaneously with an increasing number of cells (125). Starting from generation zero (g0) on the right, it is possible to read here that this assay lasted for approximately 6 days. The high peak of g0 can be explained by some dead T cells, which had lost their capability for proliferation.

3.5.3.2. Used dyes after harvesting

The subsequent use of reagents for surface antigen staining required a cooled storage of all ingredients (e.g. in an ice box); the centrifuge had been cooled down to 4 °C. Sterile conditions were not necessary.

Some samples were used as controls for compensation for flow cytometry (single-color) and only received an adapted single-color solution and thereafter remained in part unstained. One sample remained entirely unstained. These samples were instead treated with buffer solutions (PBS(-/-) or SB), so that they received the same number of treatment and washing steps equal to multicolor stained samples.

Before the algorithm of the surface antigen staining protocol (figure 12) was obeyed, each well was first carefully pipetted off directly into FACS-tubes to prevent cell loss by repeated cell transfer into different tubes (cell preparation). After thoroughly pipetting up and down, the total 200 µL of cell suspension was pulled out from each well. The 96-well plate was checked afterwards under the light microscope to ensure that all wells had been completely emptied out.

Surface antigen staining: T cell medium was removed by a washing step with 1 mL of PBS(-/-), followed by centrifuging at 500 g for 5 min at 4 °C. Supernatant was then discarded and the washing step was repeated with 200 µL of staining buffer (SB).

Next, the pellet was resuspended in 50 µL of FcBlock-SB solution, including **human FcBlock** (Human TruStain FcX™, Fc Receptor Blocking Solution, BioLegend®, #422302) solved in 1:100 ratio, and incubated for 10 min in the refrigerator at 4 °C. The FcBlock binds very specific to the end of the Fc receptor of various immune cells (such as B cells or neutrophils) to ensure that only the Fab fragment from the conjugated antibodies tie on their specific T cell antigen (epitope) (126).

Meanwhile, the antibody vials were prepared by spinning swiftly before opening up. The antibodies were admixed with the respective concentration of each antibody to SB up to 50 µL per test and added to FcBlock-SB solution up to 100 µL per test with the end concentrations as described in table 3 and 4. Single-color samples received the volume of a single antibody dye solved in SB.

After adding 50 µL of antibody-SB-solution to the sample, the cells incubated for 30 min in the dark on ice (or in the fridge at 4 °C). The tests should be exposed to as little light as possible in each work step to ensure a good response of antibody staining in the flow cytometer.

In T cell proliferation assay, the protocol for surface antigen staining was continued by centrifuging the cells for 5 min at 500 g and discarding the supernatant. A washing step was repeated twice with 200 µL of cold PBS(-/-), after which T cells were resuspended in 100 µL of cold PBS(-/-) instead of SB (containing FBS) for the ensuing FVD with **APC-eFluor780** (Allophycocyanin with eFluor™ 780; eBioscience™ Fixable Viability Dye eFluor™ 780, Thermo Fisher Scientific, #65-0865-14, LOT no. 2365397), which would have decreased staining intensity of the dead population through high protein buffers (127). Therefore, the FVD, which was frozen at -80 °C, had to be equilibrated slowly to room temperature on ice. After this step, the FVD was diluted in 1:1,000 ratio in 100 µL of PBS(-/-) per test and admixed to cell suspension to a final ratio of 1:2,000. Next,

the cell suspension incubated for 30 min on ice in the dark (or in the fridge at 4 °C).

Using FVD allows to remove dead cells from analysis, in which FVD-positive cells in the flow cytometer signal to be dead by the binding of FVD to intracellular amino acid binding sites after the loss of the cell membrane barrier (127). In the course, I removed the FVD entirely from the staining protocol.

T cells were then resuspended in 100 µL of **IC-Fixation** (eBioscience™ IC Fixation Buffer, Thermo Fisher Scientific, #00-8222-49, 2 X solution) and incubated for 10 min at 4 °C in the dark. IC-Fixation was performed, when the samples were not measured on the same day and had to be stored overnight. After adding 100 µL of SB, the cells were centrifuged and supernatant was removed. Finally, the cells were resuspended – depending on cell count – in 50 µL to 150 µL SB for the measurement. If measurement was planned for the next day, the cells were stored in the fridge; if the fixation was skipped, the cells were only washed with 100 µL SB twice.

Apoptosis dye: In T cell apoptosis assay, the apoptosis dye with **Annexin V-FITC** (BD Pharmingen™ FITC Annexin V Apoptosis Detection Kit I, BD Biosciences, #556547; FITC Annexin V, component no. 51-65874X) and **PI-PE** (BD Pharmingen™ FITC Annexin V Apoptosis Detection Kit I, BD Biosciences, #556547; Propidium Iodide Staining Solution, component no. 51-66211E) was performed after the incubation of cells with antibody-SB solution. The cells were then washed by adding 100 µL SB per test, centrifuged (500 g, 5 min, 4 °C) and washed twice with 200 µL PBS(-/-). Importantly, the supernatant was not removed by virtue of cell debris within the fluid, instead, each supernatant was gently pipetted off after centrifuging. Meanwhile, 1 X of b*inding buffer* was prepared by diluting **Annexin-binding buffer** (BD Pharmingen™ FITC Annexin V Apoptosis Detection Kit I, BD Biosciences, #556547, 10 X Annexin V Binding Buffer, component no. 51-66121E) in DI water in 1:10 ratio (600 µL per test had been prepared). Afterwards cells were resuspended in 100 µL of *binding buffer* (1 X) per test regardless of the number of cells and stained by adding each Annexin V-FITC and PI-PE to cell suspension in 1:22 ratio. The cells were agitated gently and incubated for 15 min at RT in the dark. Finally, 400 µL of *binding buffer* was added

to each tube for the analysis, which had to be done within one hour (122). It must be noted, that no cell fixation should take place in apoptosis staining.

Annexin V, as a calcium dependent phospholipid binding protein with a high affinity for (intracellular) phosphatidylserine for detection of externalization in early apoptosis, in combination with PI, as a nucleic acid dye for intercalation into the DNA for detection of late apoptosis, allows to separate early from late apoptotic cells (95,122).

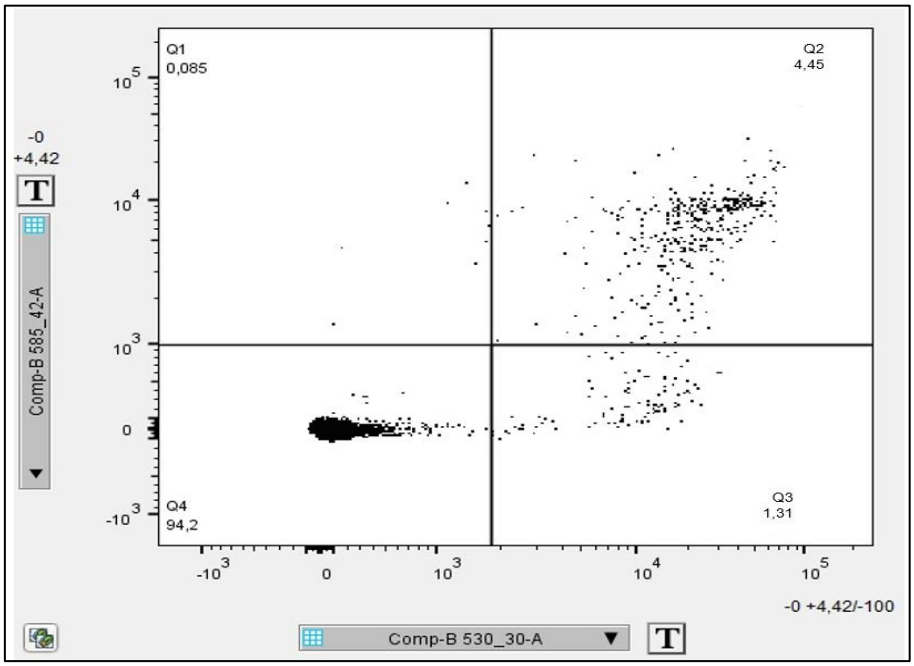

Figure 14: PI/Annexin V apoptosis dye elicited early and late apoptotic T cells.

The combination of Annexin V-FITC (B530) and PI-PE (B585) allowed to distinguish between early apoptotic and late apoptotic cells. Cells were alive when they were both negative for Annexin V and PI (lower left quadrant). At the state of externalization throughout early apoptosis, the cells were then positive for Annexin V but negative for PI (lower right quadrant). When cells were finally apoptotic and lost their membrane barrier they were then both Annexin V and PI positive (upper right quadrant) (122).

3.6. Measurement and compensation in flow cytometry

3.6.1. Preparation

3.6.1.1. Before measuring

The preparation of the measurement began with the planning of the panels. In brief, the panels were run with different and as far as possible non-interfering antibody dyes with the corresponding emission spectrum. Additional tubes were used for single antibody staining (instead of antibody capture beads) as the positive control and also one sample with unstained cells (representing an actual sample of autofluorescence) as the negative control to perform the compensation throughout the measurement. For proper compensation, controls and samples were matched, i.e. they had received both the identical treatment (except for being co-cultured with neutrophils) and the identical fluorochrome (95).

3.6.1.2. Instrument settings

The flow cytometer was prepared for the proper alignment of components to ensure that each cell travels through the apparatus separately and is exposed to the same intensity of excitation. Therefore, the fluidics, laser and settings were checked according to the producer's manuals (128) before the measurement started.

For running new experiments, the enhancement of voltage for PMTs had to be adapted to receive acceptable resolution of even weak signals. For that, single-color stained cells ran slowly through the flow cytometer with increased voltage. Thereafter the signal behavior on the selected parameters for each fluorophore was observed using the interconnected measurement software (BD FACSDiva™ Software, BD Biosciences). When accomplished, fully-stained cells ran through the system. If events would have gone off-scale, for example, the voltages of any detector had to be decreased. Afterwards, single-color stained cells ran through once more for performing the compensation. However, by using FlowJo (FlowJo®10, BD Biosciences) it was feasible to do a post-acquisitional compensation as well.

When voltages were set, the established settings were saved as a template for the next panel to ensure that the same conditions for the measurement of the respective panel were available at any time (95).

3.6.2. The actual measurement

When preparation succeeded, the experimental samples from the panel run through the instrument. To have a balanced cell count over a defined period of time, each tube was vortexed before set on the nozzle. To maintain the same measurement conditions, each sample was limited by reaching either a predefined time of 2 minutes, or a number of events of 5 x 10^4 cells.

After each measurement, the system was rinsed with the recommended fluidics (128).

3.6.3. Compensation

For the experiments, compensation was done either throughout data acquisition or post-acquisitional using a special software (FlowJo®10). When PMT voltages (FL channels) had been set, single-color stained controls with both positive and negative population ran through the cytometer, then the separate regions were drawn and displayed by the software. The compensation values were adjusted then, so that the medians of both regions matched (95), details in chapter 4.3..

3.7. Software packages

I am grateful to be able to use BioRender® by free subscription for graphical representation of the contents and used inter alia the aforementioned affiliated software of FlowJo®10 and FACSDiva™ from BD Biosciences for data analysis.

3.8. Data processing

Neutrophil shape change data were analyzed using Microsoft Excel 2016 (Microsoft Corporation) and by comparing vehicle vs. different IL-8 concentrations (0.04-10 nM).

Flow cytometry was performed for evaluating aberrant T cell proliferation or aggravated T cell apoptosis by the presence of neutrophils *in vitro*. Data were compiled in Excel worksheets and analyzed in SPSS (IBM, SPSS Statistics, v.27). For graphical representation, GraphPad PRISM (GraphPad Software, Inc., v. 5.01) was used.

3.9. Statistics

SPSS was used for statistical analysis. T cell proliferation and T cell apoptosis data were assessed for Gaussian distribution by Shapiro-Wilk. One-way ANOVA was used as the parametric test, and for non-parametric data (Gaussian approximation) Kruskal-Wallis tests was performed. For both tests the factor (independent variable) with its different groups was set as treatment with neutrophils (“A549, B2B, naïve”) including one group without neutrophils (“CD3+ only”) as negative control.

The mean across the different groups of all parametric data were tested for homogeneity of variances with Levene’s test as part of one-way ANOVA, where a p-value > 0.05 was observed in all tests. In case of statistical significance post-hoc tests would have been performed. In the Kruskal-Wallis test the number of samples was < 30 and required therefore the exact significance and/or the pairwise comparison of independent samples. However, in case of no statistical significance these steps would have become dispensable.

In all analyses, a p-value of ≤ 0.05 fulfilled the criterion to be referred as statistically significant.

4. Results

4.1. Neutrophil activation upon IL-8 stimulation behaved in a similar fashion using naïve neutrophils and neutrophils recovered from the eosinophil isolation protocol

To ascertain the usability of isolated neutrophils in terms of their preserved cell integrity, a neutrophil shape change assay was performed.

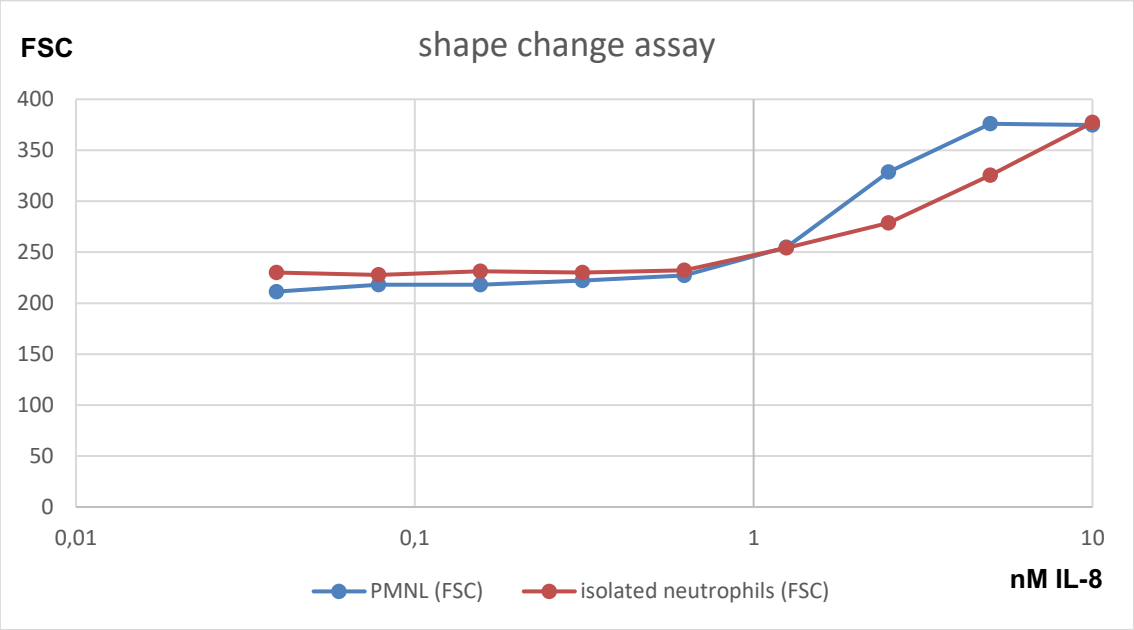

Figure 15: Identical dose response curves in PMNL and isolated neutrophils upon IL-8 stimulation.

Increasing concentrations (0.04 to 10 nM) of IL-8 induced neutrophil shape change measured by FSC properties using flow cytometry. Neutrophils (PMNL faction, blue line) and isolated neutrophils (red line) were compared, and no difference was observed. This graph represents one experiment, thus no statistical analysis was performed.

4.2. Stain indices from APC and PE topped the ranking, whereas SI from eF450 proliferation dye and FITC as part of apoptosis dye were less bright

Stain indices from the used fluorophores were compared using the information from websites of suppliers (129,130) to ascertain the brightest fluorophores (high SI) for low-density antigens and vice versa.

As part of the experimental setup, different titrations and antibody dyes and combinations were tried out. Nevertheless, best conditions were experienced by fluorophores from table 5.

Table 5: Stain indices from the used fluorophores in the panels.

Reagent	fluorescence channel	**Filters**	**Excitation** maximum	**Emission** maximum	**Stain index**
abbreviation of dye		wavelengths in nm			dimensionless or as rating(*)
FITC	FL1	BP 530/30	490-494	515-525	(*3)
PE	FL2	BP 585/45	565-566	576-578	158 (*1)
PE-Cy7	FL4	BP 780/60	565-566	774-781	(*2)
APC	FL5	BP 660/20	650-651	660	200 (*1)
APC-eFluor780	FL6	BP 780/60	655	780	(*4)
eFluor450	FL7	BP 450/50	405	450	(*4)

The used reagents with their stain indices based on the available lasers and filters of the flow cytometer (BD FACSCanto™ II) – the colored background represents the color of the laser (131).

Suppliers of fluorescent dyes typically provide a brightness ranking of 1 (very bright) to 5 (dim) for each label in their catalog. The ranking varies from supplier to supplier owing to their different rating criteria (129,130,132,133). The stain indices listed above stem from the website of Thermo Fisher Scientific (130) and was compared to information from the website of BD Biosciences (129). APC and PE topped the ranking in terms of their brightness, PE-Cy7 was moderate, all others were less bright. BP filters = band pass filters.

4.3. Compensation was done properly only, when the median fluorescence of the false-positives was equal to the median fluorescence of the negatives

Compensation was performed to receive an accurate distinction of a single fluorochrome in the presence of two or more fluorochromes due to their physical property of interfering with adjacent emission spectra (96,134,135).

Overlapping fluorescent signals, which were not only detected correctly by one channel (FL1) but also detected wrongly by a second channel (FL2), were subtracted out and could be simplified by following equation:

$FL2_{true} = FL2_{measured} – x\ \%\ FL1_{measured}$ (134,135)

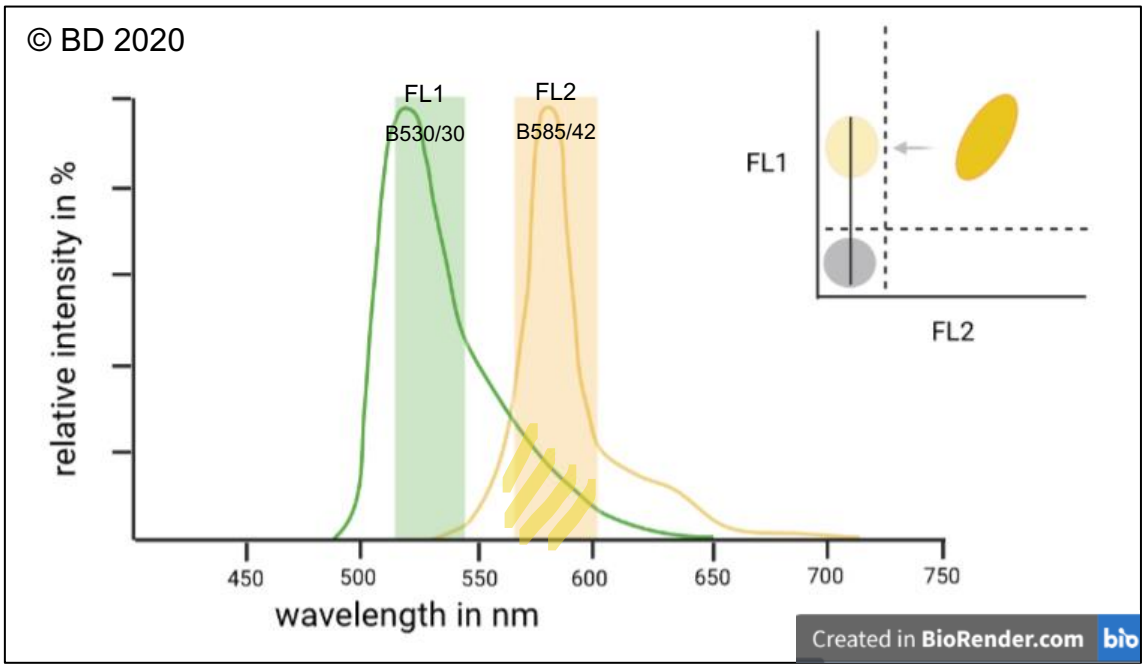

Figure 16: Emission overspill and compensation for the FL2 channel.

FITC in green and PE in yellow are sketched above with their emission spectra and emission overspills. FITC overlaps into the wrong channel (FL2) more than PE does (into FL1) by virtue of low green emission spectrum. Both overspills must be taken into account and must be compensated by subtraction. Figure was reproduced with permission of BD Biosciences (96).

Figures 17-21 show the impact of the subtraction of emission overspill from FITC into PE-channel (FL2) until it was done properly.

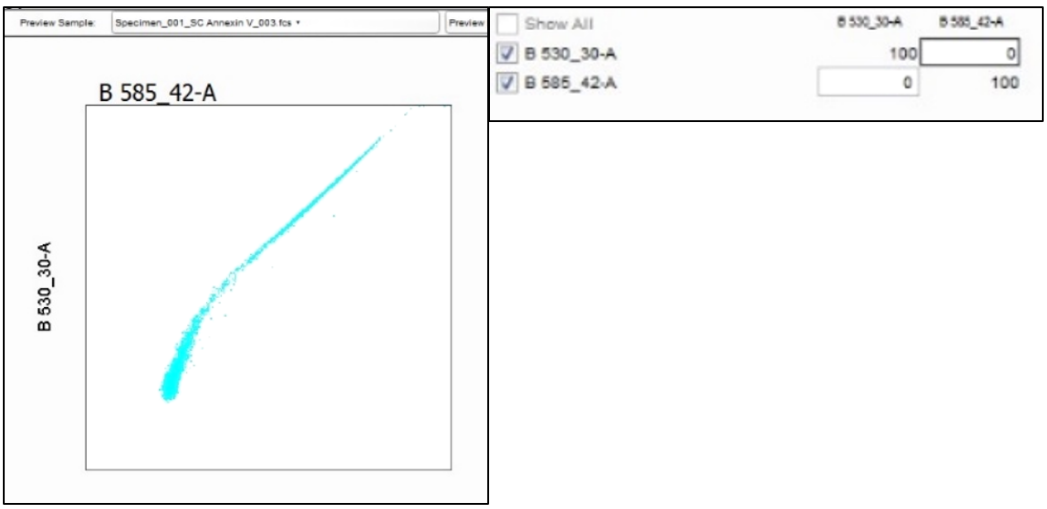

Figure 17: Uncompensated single-color stained sample (FL2 = FL2 – 0% FL1).

In this example, apoptosis dye was conducted inter alia with Annexin V-FITC (equate with B530/30) and PI-PE (equate with B585/42); the FL1 channel is represented by B530/30-A and the FL2 channel by B585/42-A (in fact the FL2 channel in BD FACSCanto™ II is equipped with the filter 585/45). The 'A' after the number of filter describes the 'area' under the curve (integral) of the emission that is detected by the filter.

Figures 17-21 stem from a sample of T cell apoptosis assay and were edited post-acquisitional using FlowJo.

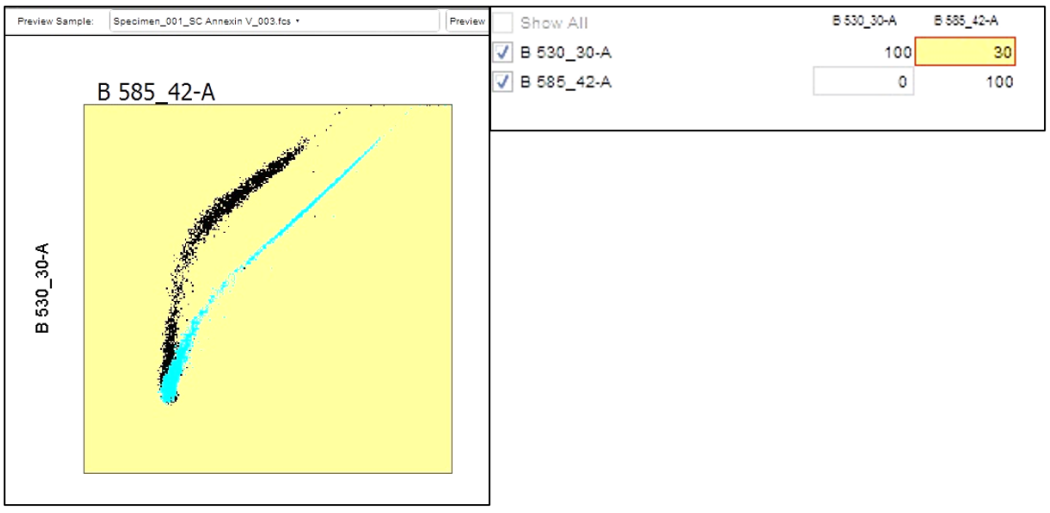

Figure 18: Undercompensated single-color stained sample (FL2 = FL2 – 30% FL1).

The grid above shows the percentage of subtraction of the measured intensity in channel FL1 (B530/30) from channel FL2 (B585/42). In this case, there was still undercompensation, where parts of the cells could still be found in the FL2-positive (B585/42) area.

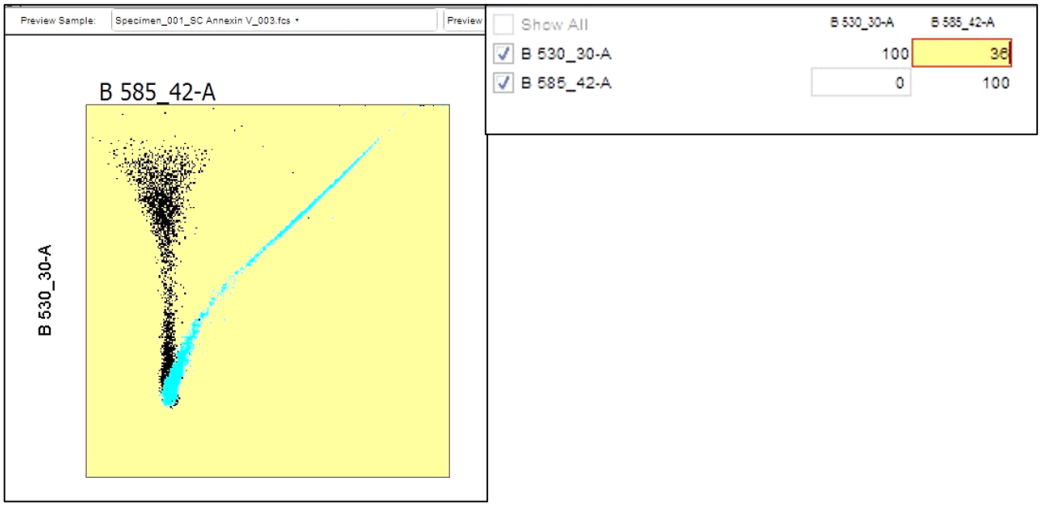

Figure 19: Overcompensated single-color stained sample (FL2 = FL2 – 36% FL1).

Parts of the cells came into the negative area of FL2 and can be considered as loss of signals.

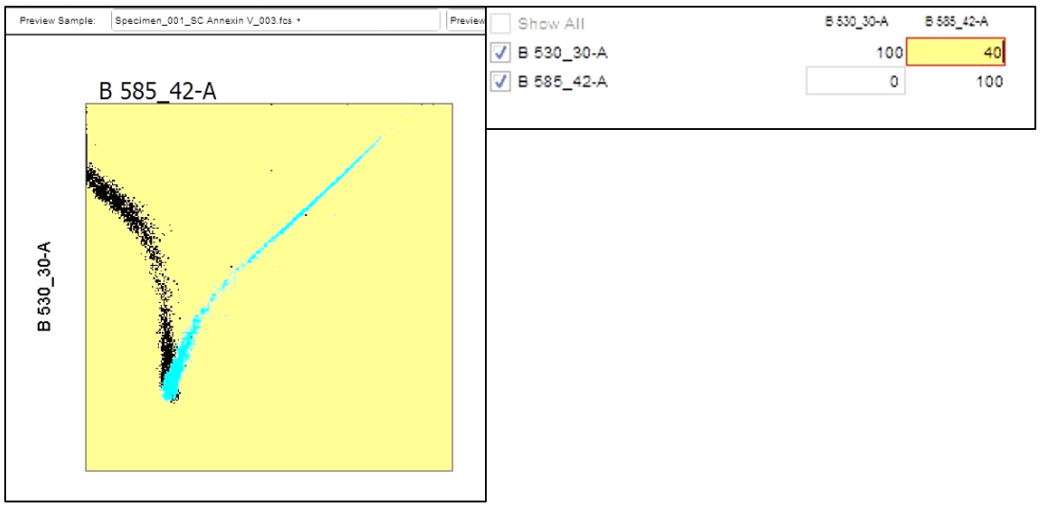

Figure 20: Highly overcompensated single-color stained sample (FL2 = FL2 – 40% FL1).

Merely 4% had been additionally subtracted compared to figure 19, which resulted in a vast loss of signals by shifting into the negative area of FL2 and going off-scale.

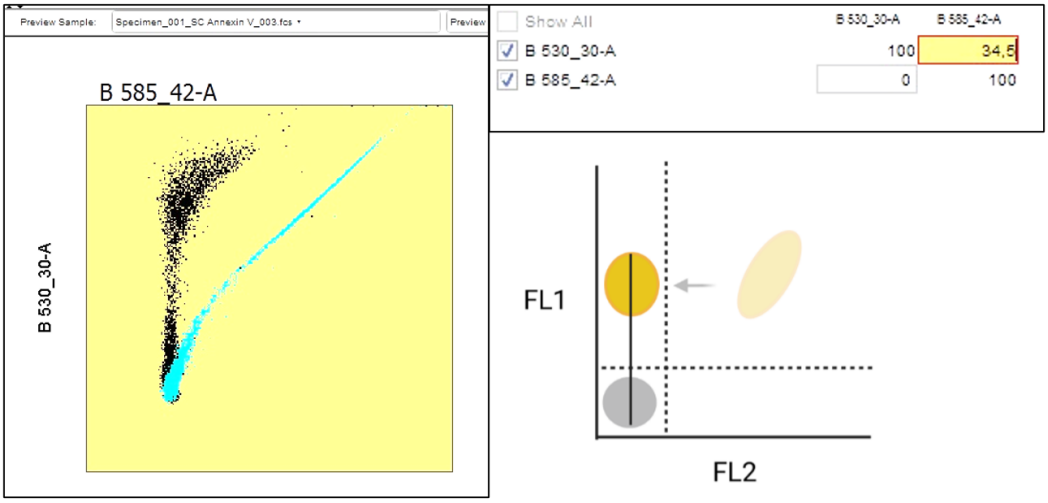

Figure 21: Properly compensated single-color stained sample (FL2 = FL2 – 34.5% FL1).

The medians of both the negative population and FITC-positive population had been adjusted and were lined up.

Compensation values from single-color stained samples of all applied fluorophores within a panel had been transferred to each multicolor sample, and are represented in figures 23 and 27 below, which were performed post-acquisitional using FlowJo.

4.4. No differences in generation zero of T cells after co-culturing with stimulated neutrophils compared to T cells in mono-culture

To ascertain an aberrant proliferation behavior of T cells in the presence of neutrophils (in 5:1 ratio), cells were co-cultured for three and six days. Additionally, neutrophils were stimulated with cell supernatants (A549 and B2B in 1:1 or 1:20 dilution) or remained untreated (naïve). For control, a mono-culture of T lymphocytes (CD3+ only) was conducted simultaneously. The T cell proliferation assay contained an experimental series with four samples, where all groups underwent the same conditions in culturing and staining, and were targeted to elicit generation zero (g0) – the fraction in which no proliferation occurred – for $CD4^+$ and $CD8^+$ cells.

Figure 22: Expected emission spectra of a multicolor panel for proliferation dye and surface antigen staining in T cell proliferation assay (123,131,136).

In accordance with the settings of the flow cytometer, the single dyes were markedly delimited and showed few overlaps concerning the different filters (bigger overspill through FITC). However, at first glance, the selection looked useable. The FVD (APC-eFluor780) showed no overspill with another filter due to its property of emitting light into far red regions. Blue = eFluor450; green = FITC; yellow = PE; dark red = APC-eFluor780.

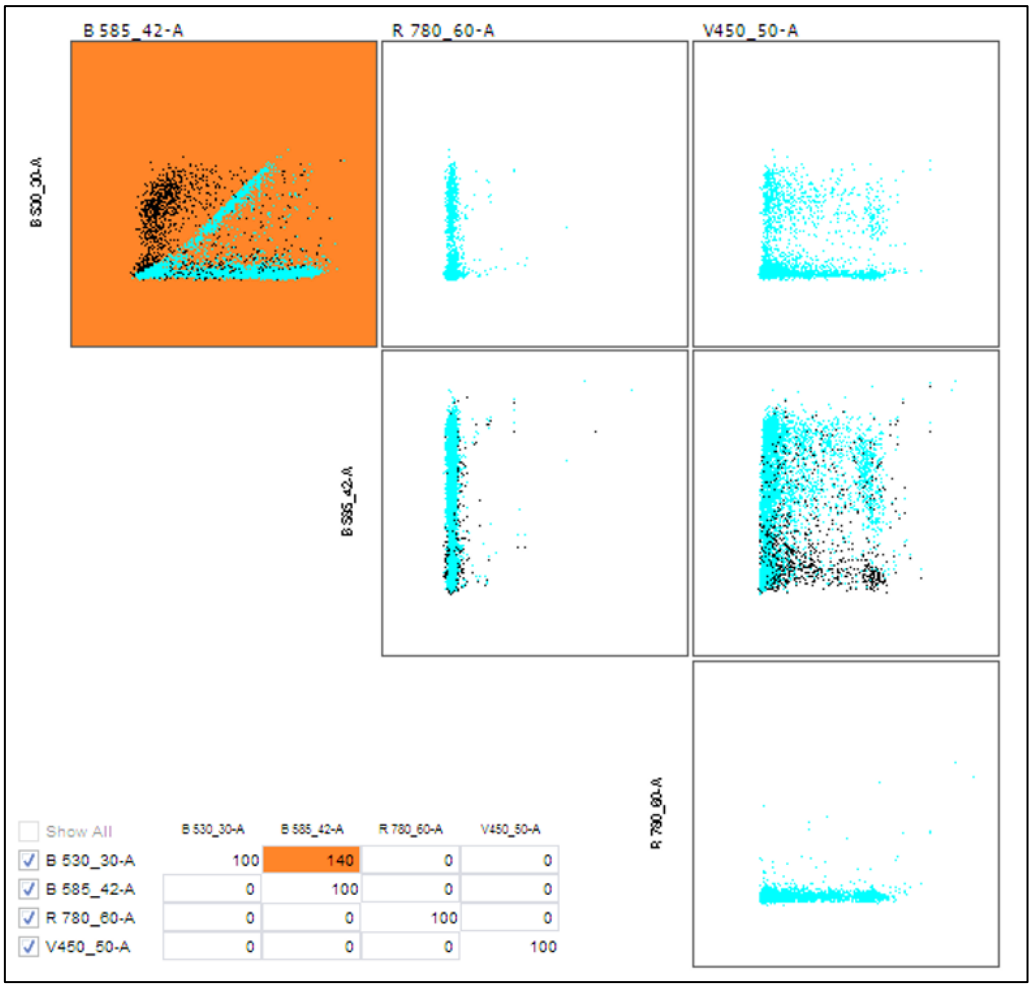

Figure 23: Representative compensation matrix of the multicolor panel in the T cell proliferation assay.

A compensation value of 140 was applied to compensate false positive signals from FITC out of the PE channel.

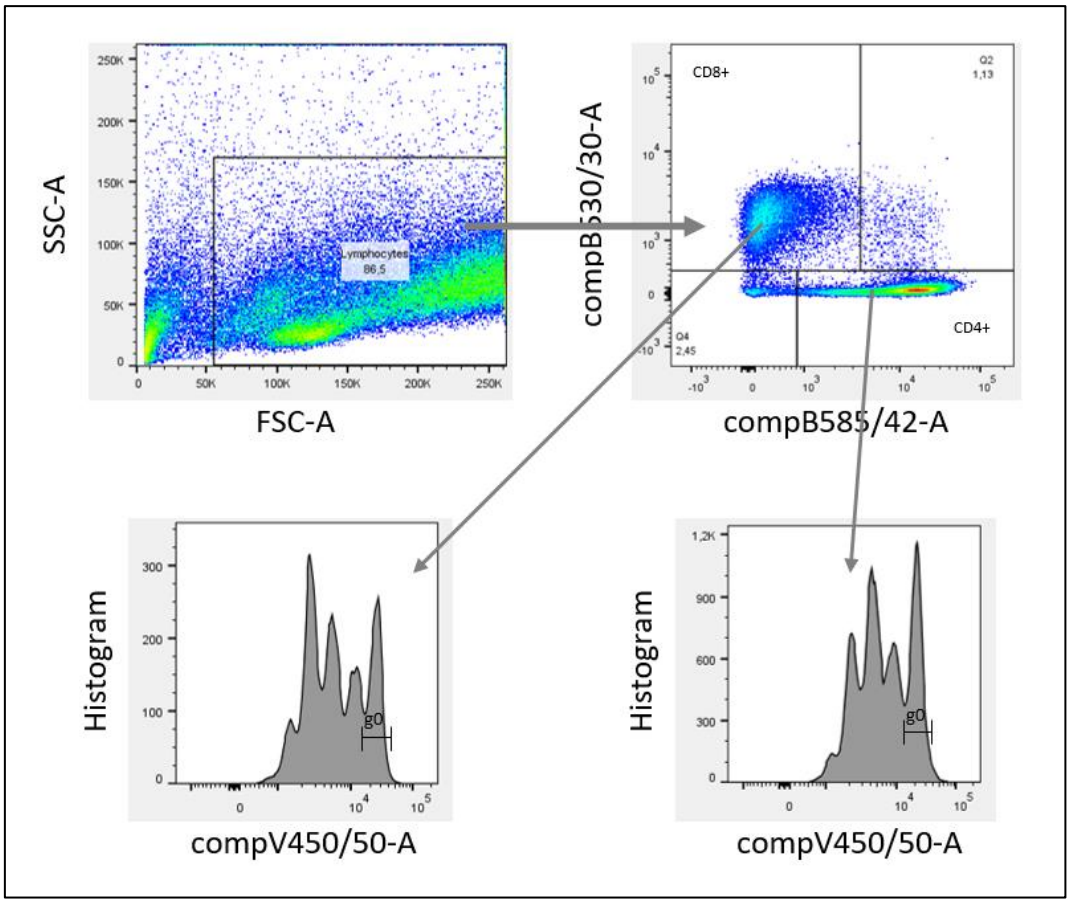

Figure 24: Flow gating of the multicolor panel in the T cell proliferation assay.

In the T cell proliferation assay, the main population was identified (fraction consisting of T lymphocytes) using FSC-A and SSC-A. The population was then divided into CD4-positives and CD8-positives by detecting their respective staining (PE, FITC), whereafter both were finally examined concerning their proliferation behavior through eF450 proliferation dye and gated using a range gate to ascertain the percentage of generation zero (g0).

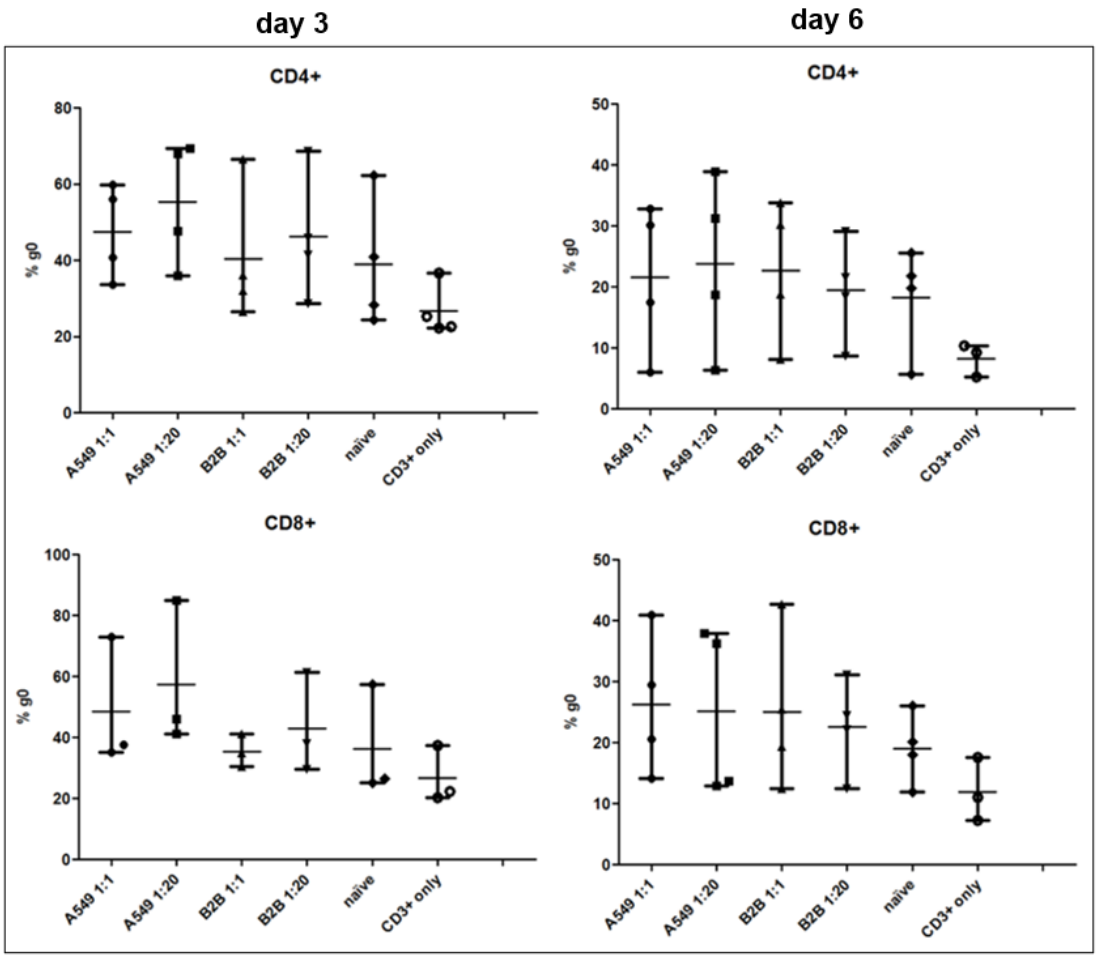

Figure 25: Percentages of generation zero in CD4⁺ and CD8⁺ T cells at day 3 and day 6.

One-way ANOVA found no statistically significant differences between the mean percentages of g0 in CD4⁺/day3 (n=24, p=0.194, F=1.663), CD4⁺/day6 (n=23, p=0.495, F=0.914), CD8⁺/day3 (n=18, p=0.356, F=1.224) or CD8⁺/day6 (n=23, p=0.493, F=0.918) with/without neutrophils. The control group ("CD3+ only") is characterized by having the lowest percentages of g0 and showing the highest proliferation rates. Low proliferation rates were more often pronounced in the groups with A549 1:20 and B2B 1:20 than in A549 1:1 and B2B 1:1. Each dot represents an independent data point as determined by flow cytometry. Data are presented as mean with range.

4.5. No differences in apoptosis counts of T cells after co-culturing with stimulated neutrophils compared to T cells in mono-culture

To ascertain an aggravated number of T cell apoptosis in the presence of neutrophils (in 5:1 ratio), both cell fractions had been co-cultured for 24 hours. Apart from that, the conditions were equal to those of the T cell proliferation assay. For this assay, an experimental series with again four samples was conducted and targeted the early and late apoptosis counts in $CD4^+$ and $CD8^+$ cells.

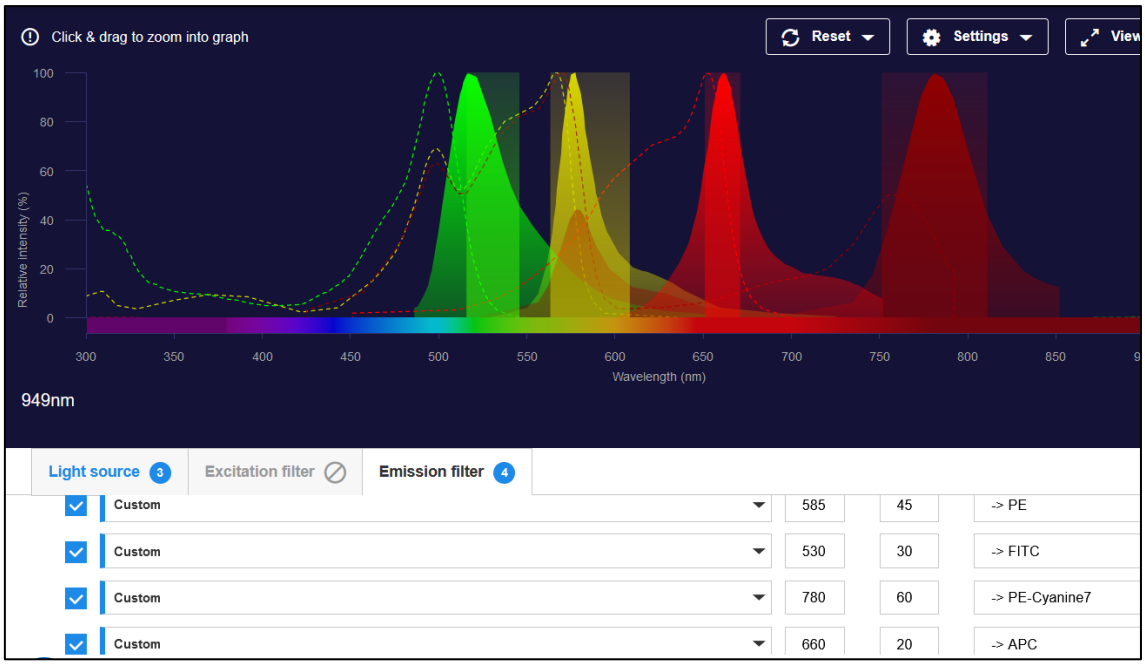

Figure 26: Expected emission spectra of a multicolor panel for apoptosis dye and surface antigen staining in the T cell apoptosis assay (123,131,136).

Many overlaps, typically by PE and FITC, but especially for the PE filter a greater interference with PE-Cy7 could be observed. However, it was not feasible without PE and FITC, since both were used for apoptosis detection (PI and Annexin V), hence a possible corresponding distortion in measuring data was assumed, where compensation must be done properly. Green = FITC; yellow = PE; red = APC; dark red = PE-Cy7.

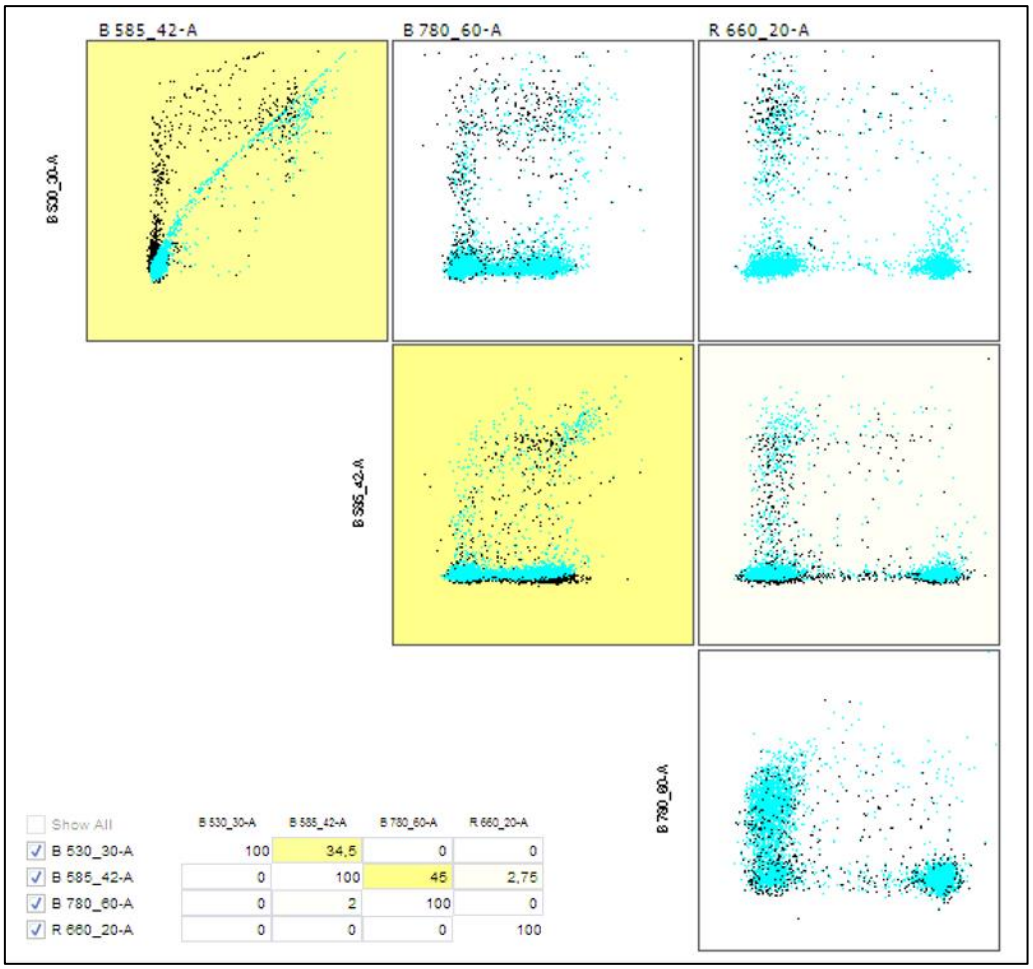

Figure 27: Representative compensation matrix of the multicolor panel in the T cell apoptosis assay.

Here, the compensation of FITC occurred as expected as well as the vast overspill from PE-Cy7 into the PE channel due to its composition as tandem dye with 'PE' (figure 26). Nevertheless, the positive signals could be delimited well from the negatives after compensation.

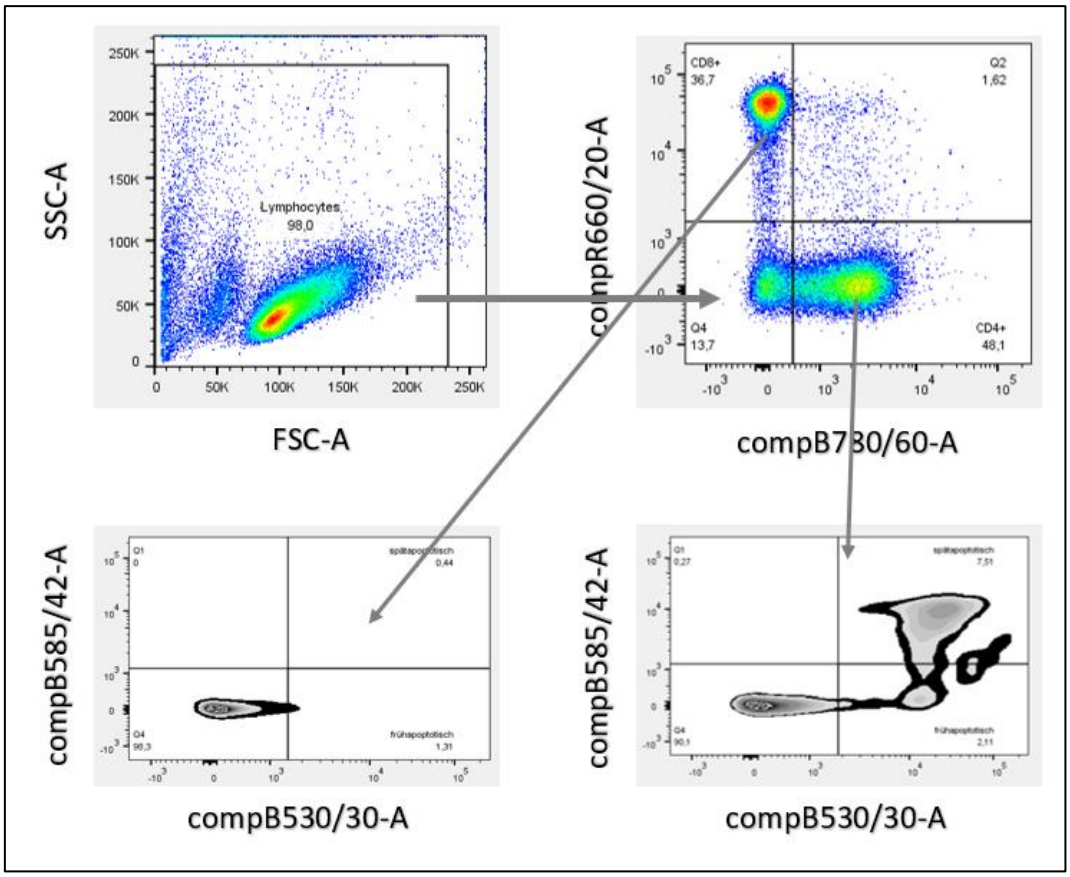

Figure 28: Flow gating of the multicolor panel in the T cell apoptosis assay.

In the T cell apoptosis assay, all T cells, dead or alive, were included as opposed to the aforementioned proliferation assay. Those were then distinguished into CD4-positives and CD8-positives by detecting their respective dye (PE-Cy7, APC). Thereafter the apoptosis behavior of both was examined using PI/Annexin V apoptosis dye (PE, FITC).

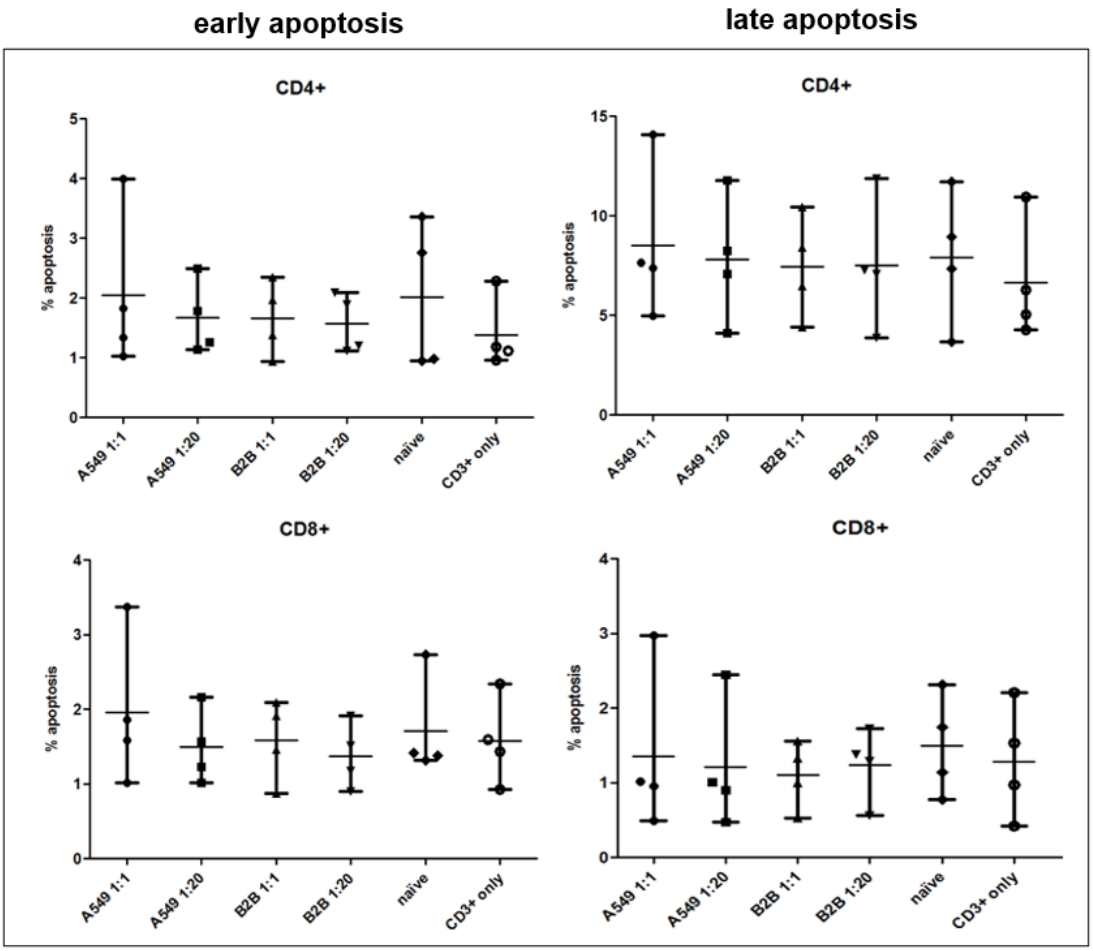

Figure 29: Percentages of early and late apoptosis counts in CD4⁺ and CD8⁺ T cells.

Testing the differences of the mean percentages with one-way ANOVA did not achieve to statistical significance in CD4⁺/early apoptosis (n=24, p=0.881, F=0.341), CD4⁺/late apoptosis (n=24, p=0.978, F=0.149) and CD8⁺/late apoptosis (n=24, p=0.985, F=0.124). Kruskal-Wallis test used for CD8⁺/early apoptosis found no statistically significant differences (n=24, asymptotic significance=0.945, Kruskal-Wallis statistic=1.196) between the groups. Almost all groups have the identical mean percentage level. The group of A549 1:1 was constantly responsible for the highest numeric apoptosis. Heightened absolute percentages of late apoptosis in CD4⁺ can be observed. Each dot represents an independent data point as determined by flow cytometry. Data are presented as mean with range.

5. Discussion

The interaction between T cells and neutrophils is a far more complex phenomenon that cannot be explained by these experiments, at best observed indirectly throughout the analysis of T cells. However, the experiments tended that T cell proliferation was impaired by co-culturing with neutrophils as opposed to proper proliferation generations in mono-cultured T cells (figure 25). Presumably, even the mere fact that the presence of another leukocyte faction in human T cell culture is sufficient for disruption of the physiological cell cycle in T cells.

With the different treatments of neutrophils the highest disruption of both T cell proliferation and T cell apoptosis was expected by A549, followed by B2B in their respective descending concentrations, and then by naïve neutrophils. I was particularly curious about eventual differences in $CD4^+$ and $CD8^+$ cells. Indeed, the differences were only small; in T cell proliferation the highest distortion may be assigned to A549 1:20 for both $CD4^+$ and $CD8^+$ cells (figure 25); whereas in T cell apoptosis A549 1:1 was the leading factor for high apoptosis counts irrespective of the T cell subset (figure 29). However, there is the trend that $CD4^+$ cells were prone to have elevated counts in late apoptotic cells (figure 29), which may be assigned to a higher susceptibility of $CD4^+$ cells to neutrophils already in the early encounter.

The methods seem to be able to deliver statements for proliferation behavior as to apoptosis counts where in the latter almost all groups remained indistinctly affected by co-culturing (figure 29). Differences in apoptosis counts were observed in a preliminary experiment by merely shifting the ratio between T cells (PBMCs) and neutrophils in favor of the neutrophils. Likewise, the treatment with cell supernatants delivered differences concerning a decreased proliferation rate and deteriorated viability especially when neutrophils were treated with A549 in higher concentration (figure 25). Nonetheless it has to be taken into consideration that too high concentrations of supernatants – especially a 1 to 1 ratio – in A549 as well as B2B delivered contradictory results (figures 25 and 29), presumably due to cytotoxic effects on neutrophils, compared to concentrations of only a twentieth. Regarding the viability of neutrophils, the importance of the physiological mean retention time *in vivo* of eight hours in blood and after a possible migration into tissue a mean survival time of one to two days (137) must be taken into account

as well, consequently an indirect proportionality between neutrophil viability and duration of neutrophil treatment *in vitro* should be expected.

Regarding the composition of the T cell medium in the T cell apoptosis assay, FBS was halved to an end concentration in the medium of 5 Vol.% in the assumption that FBS reduces the enzyme activity of neutrophils, especially in the first hours in co-culture. This would have had an adverse effect on their functionality within the relatively short-term culturing of 24 hours. However, T cells could not without FBS – for this reason FBS was merely reduced and not completely removed from the T cell medium. In the course of the experimental setup, RPMI and FBS could be replaced by XVivo15 and it was possible to renounce entirely the FBS.

Based on these observations, the method for T cell proliferation apparently worked better and was more promising than the method for T cell apoptosis, even if both failed the statistical tests. Throughout this relatively short time for the diploma thesis, it was not realizable to conduct more samples for the statistics. Nevertheless, it would be useful to perfect the aforementioned methods and performed them at least five times. Perfecting would involve the exclusion of any potential source of error, starting with the selection of proper/neutral material, e.g. DMEM in cell supernatants, since those still contained FBS as an inhibitor for neutrophil enzymes, for instance, and could explain the paradoxical results in A549 or B2B groups. On the other hand, it would not have been feasible to perform tumor cell culturing without DMEM. Next, it is important to properly select antibody dyes with higher SI to reduce high compensation values and select of as low as necessary titration to avoid unspecific binding by vast excess of antibody dye to antigens. This may be represented by a simple calculation example: Approximately 5×10^4 CD4 molecules are attached per T cell; by an approach with 2.5×10^5 T cells there would be 12.5×10^9 CD4 molecules to stain. Following the supplier's recommendation to stain with 1 µL of CD4-antibody dye per 100 µL we would stain 1.8×10^{12} CD4 molecules. Accordingly, the 144-fold excess, albeit the 5-fold excess would be sufficient (95), what could be then transferred (theoretically) in an amount of merely ~17.5 nL per test. Optimizing the work processes would include the instrument settings as well, where compensation had to be set anew each time when the instrument is running, since the machine is slightly different each time when it warms up (95). Besides, this is substantiated by

the fact that high voltages and compensation values deliver rather impure data. Generally, the established methods may encompass theoretically a myriad number of possibilities for pitfalls. On the other hand, even if each work step would be performed under optimal conditions the results might be equal to those described above.

With all these considerations I still hypothesize that the interaction between neutrophils and T lymphocytes is characterized by a negative correlation. However, in this study of only a few samples (four experiments per method maximum) the p-value suffered and led to statistically non-significant results.

To conclude, none of the aforementioned methods were statistically significant to make safe statements about impaired T cell proliferation behavior in the presence of neutrophils or an aggravated number of T cell apoptosis. The hypothesis remains unsolved in terms of the human model. It only can be said that the methods for examining this hypothesis did not work as expected – accordingly double-edged as known from literature – and merely delivered further clues that T lymphocytes might be impaired in their function in the vicinity of another leukocyte fraction throughout co-culturing, and in particular that $CD4^+$ cells might be more susceptible to lethal disruption by neutrophils already in the early encounter.

6. References

(1) Aigner KR, Stephens FO, Allen-Mersh T, Hortobagyi G, Khayat D, Picksley SM, et al. Lungenkrebs (Bronchialkarzinom). In: K. R. Aigner, F. O. Stephens, editor. Onkologie Basiswissen Berlin Heidelberg: Springer-Verlag; 2016. p. 127-132.

(2) Herold G, et al. III. Pneumologie, Lungenkarzinom. In: Dr. med. Gerd Herold, editor. Innere Medizin. 2020th ed. Köln, DE; 2020. p. 400-406.

(3) Griesinger F, Absenger G, Eberhardt W, Früh M, Gautschi O, Hilbe Wea. Lungenkarzinom, nicht-kleinzellig (NSCLC). Jul/2021; Available at: https://www.onkopedia.com/de/onkopedia/guidelines/lungenkarzinom-nicht-kleinzellig-nsclc/@@guideline/html/index.html. Accessed Dec/2021.

(4) Statistik Austria. Luftröhre, Bronchien, Lunge. Jan/2022; Available at: https://www.statistik.at/web_de/statistiken/menschen_und_gesellschaft/gesundheit/krebserkrankungen/luftroehre_bronchien_lunge/index.html#:~:text=2019%20erkrankten%202.770%20M%C3%A4nner%20und,1.641%20Frauen%20verstarben%20zuletzt%20daran. Accessed Feb2022.

(5) American Lung Association. Lung cancer fact sheet. May/2020; Available at: https://www.lung.org/lung-health-diseases/lung-disease-lookup/lung-cancer/resource-library/lung-cancer-fact-sheet#:~:text=The%20lung%20cancer%20five%2Dyear,and%20prostate%20(98.2%20percent).&text=The%20five%2Dyear%20survival%20rate,localized%20(within%20the%20lungs). Accessed Feb/2022.

(6) Inamura K. Lung cancer: understanding its molecular pathology and the 2015 WHO classification. Front Oncol 2017 Aug 28;7:193.

(7) Travis WD. Pathology of lung cancer. Clin Chest Med 2011 Dec;32(4):669-692.

(8) Goldstraw P, Chansky K, Crowley J, Rami-Porta R, Asamura H, Eberhardt WE, et al. The IASLC lung cancer staging project: Proposals for revision of the TNM stage groupings in the forthcoming (Eighth) edition of the TNM classification for lung cancer. J Thorac Oncol 2016 Jan;11(1):39-51.

(9) Felip E, Altorki N, Zhou C, Csőszi T, Vynnychenko I, Goloborodko O, et al. Adjuvant atezolizumab after adjuvant chemotherapy in resected stage IB-IIIA non-small-cell lung cancer (IMpower010): a randomised, multicentre, open-label, phase 3 trial. Lancet 2021 Oct 9;398(10308):1344-1357.

(10) Reck M, Rodríguez-Abreu D, Robinson AG, Hui R, Csőszi T, Fülöp A, et al. Updated analysis of KEYNOTE-024: pembrolizumab versus platinum-based chemotherapy for advanced non-small-cell lung cancer with PD-L1 tumor proportion score of 50% or greater. J Clin Oncol 2019 Mar 1;37(7):537-546.

(11) Herbst RS, Giaccone G, de Marinis F, Reinmuth N, Vergnenegre A, Barrios CH, et al. Atezolizumab for first-line treatment of PD-L1-selected patients with NSCLC. N Engl J Med 2020 Oct 1;383(14):1328-1339.

(12) Paz-Ares L, Ciuleanu TE, Cobo M, Schenker M, Zurawski B, Menezes J, et al. First-line nivolumab plus ipilimumab combined with two cycles of chemotherapy in patients with non-small-cell lung cancer (CheckMate 9LA): an international, randomised, open-label, phase 3 trial. Lancet Oncol 2021 Feb;22(2):198-211.

(13) West H, McCleod M, Hussein M, Morabito A, Rittmeyer A, Conter HJ, et al. Atezolizumab in combination with carboplatin plus nab-paclitaxel chemotherapy compared with chemotherapy alone as first-line treatment for metastatic non-squamous non-small-cell lung cancer (IMpower130): a multicentre, randomised, open-label, phase 3 trial. Lancet Oncol 2019 Jul;20(7):924-937.

(14) Socinski MA, Jotte RM, Cappuzzo F, Orlandi F, Stroyakovskiy D, Nogami N, et al. Atezolizumab for first-line treatment of metastatic nonsquamous NSCLC. N Engl J Med 2018 Jun 14;378(24):2288-2301.

(15) Frost N, Zhamurashvili T, von Laffert M, Klauschen F, Ruwwe-Glösenkamp C, Raspe M, et al. Pemetrexed-based chemotherapy is inferior to Pemetrexed-free regimens in thyroid transcription factor 1 (TTF-1)-negative, EGFR/ALK-negative lung adenocarcinoma: A propensity score matched pairs analysis. Clin Lung Cancer 2020 Nov;21(6):e607-e621.

(16) Paz-Ares L, Luft A, Vicente D, Tafreshi A, Gümüş M, Mazières J, et al. Pembrolizumab plus chemotherapy for squamous non-small-cell lung cancer. N Engl J Med 2018 Nov 22;379(21):2040-2051.

(17) Topalian SL, Hodi FS, Brahmer JR, Gettinger SN, Smith DC, McDermott DF, et al. Safety, activity, and immune correlates of anti-PD-1 antibody in cancer. N Engl J Med 2012 Jun 28;366(26):2443-2454.

(18) Kargl J, Busch SE, Yang GH, Kim KH, Hanke ML, Metz HE, et al. Neutrophils dominate the immune cell composition in non-small cell lung cancer. Nat Commun 2017 Feb 1;8:14381.

(19) Strobl H. Vorlesung, Pathophysiologie des Immunsystems. 2021; Available at: https://vmc.medunigraz.at/moodle/pluginfile.php/126442/mod_resource/content/1/Pathophysiologie%20des%20Immunsystems%20SS2021%20Prof.Stobl.pdf. Accessed Dec/2021.

(20) Abbas AK, Lichtman A, Pillai S. Cellular and molecular immunology. 9th ed. Philadelphia: Elsevier; 2017.

(21) Kreuzer KA, Hallek M. Kapitel 15, Blut, physiologische Grundlagen. In: Blum HE, Müller-Wieland D, editors. Klinische Pathophysiologie. 10th ed. DE: Georg Thieme Verlag; 2018. p. 517-518.

(22) Maecker HT, McCoy JP, Nussenblatt R. Standardizing immunophenotyping for the Human Immunology Project, figure 2: identification of immunce cell subsets by eight-colour antibody staining. Nat Rev Immunol 2012 Feb 17;12(3):191-200.

(23) Zola H, Swart B, Banham A, Barry S, Beare A, Bensussan A, et al. CD molecules 2006--human cell differentiation molecules. J Immunol Methods 2007 Jan 30;319(1-2):1-5.

(24) Lüllmann R, Asan E. Kapitel 12, Blutbildung. In: Lüllmann R, editor. Taschenlehrbuch Histologie. 5th ed. Stuttgart: Georg Thieme Verlag; 2015. p. 319-321.

(25) Manz MG, Boettcher S. Emergency granulopoiesis. Nat Rev Immunol 2014 May;14(5):302-314.

(26) Hanahan D, Weinberg RA. Hallmarks of cancer: the next generation. Cell 2011 Mar 4;144(5):646-674.

(27) Yang L, Pang Y, Moses HL. TGF-beta and immune cells: an important regulatory axis in the tumor microenvironment and progression. Trends Immunol 2010 Jun;31(6):220-227.

(28) Shields JD, Kourtis IC, Tomei AA, Roberts JM, Swartz MA. Induction of lymphoidlike stroma and immune escape by tumors that express the chemokine CCL21. Science 2010 May 7;328(5979):749-752.

(29) Ostrand-Rosenberg S, Sinha P. Myeloid-derived suppressor cells: linking inflammation and cancer. J Immunol 2009 Apr 15;182(8):4499-4506.

(30) Mougiakakos D, Choudhury A, Lladser A, Kiessling R, Johansson CC. Regulatory T cells in cancer. Adv Cancer Res 2010;107:57-117.

(31) Bergers G, Benjamin LE. Tumorigenesis and the angiogenic switch. Nat Rev Cancer 2003 Jun;3(6):401-410.

(32) Baeriswyl V, Christofori G. The angiogenic switch in carcinogenesis. Semin Cancer Biol 2009 Oct;19(5):329-337.

(33) Zumsteg A, Christofori G. Corrupt policemen: inflammatory cells promote tumor angiogenesis. Curr Opin Oncol 2009 Jan;21(1):60-70.

(34) Qian BZ, Pollard JW. Macrophage diversity enhances tumor progression and metastasis. Cell 2010 Apr 2;141(1):39-51.

(35) Murdoch C, Muthana M, Coffelt SB, Lewis CE. The role of myeloid cells in the promotion of tumour angiogenesis. Nat Rev Cancer 2008 Aug;8(8):618-631.

(36) De Palma M, Murdoch C, Venneri MA, Naldini L, Lewis CE. Tie2-expressing monocytes: regulation of tumor angiogenesis and therapeutic implications. Trends Immunol 2007 Dec;28(12):519-524.

(37) Cavallaro U, Christofori G. Cell adhesion and signalling by cadherins and Ig-CAMs in cancer. Nat Rev Cancer 2004 Feb;4(2):118-132.

(38) Berx G, van Roy F. Involvement of members of the cadherin superfamily in cancer. Cold Spring Harb Perspect Biol 2009 Dec;1(6):a003129.

(39) Palermo C, Joyce JA. Cysteine cathepsin proteases as pharmacological targets in cancer. Trends Pharmacol Sci 2008 Jan;29(1):22-28.

(40) Mohamed MM, Sloane BF. Cysteine cathepsins: multifunctional enzymes in cancer. Nat Rev Cancer 2006 Oct;6(10):764-775.

(41) Joyce JA, Pollard JW. Microenvironmental regulation of metastasis. Nat Rev Cancer 2009 Apr;9(4):239-252.

(42) Kessenbrock K, Plaks V, Werb Z. Matrix metalloproteinases: regulators of the tumor microenvironment. Cell 2010 Apr 2;141(1):52-67.

(43) Karnoub AE, Weinberg RA. Chemokine networks and breast cancer metastasis. Breast Dis 2006 -2007;26:75-85.

(44) Grivennikov SI, Greten FR, Karin M. Immunity, inflammation, and cancer. Cell 2010 Mar 19;140(6):883-899.

(45) DeNardo DG, Andreu P, Coussens LM. Interactions between lymphocytes and myeloid cells regulate pro- versus anti-tumor immunity. Cancer Metastasis Rev 2010 Jun;29(2):309-316.

(46) Vajdic CM, van Leeuwen MT. Cancer incidence and risk factors after solid organ transplantation. Int J Cancer 2009 Oct 15;125(8):1747-1754.

(47) Teng MW, Swann JB, Koebel CM, Schreiber RD, Smyth MJ. Immune-mediated dormancy: an equilibrium with cancer. J Leukoc Biol 2008 Oct;84(4):988-993.

(48) Schäfer M, Werner S. Cancer as an overhealing wound: an old hypothesis revisited. Nat Rev Mol Cell Biol 2008 Aug;9(8):628-638.

(49) Chung AS, Wu X, Zhuang G, Ngu H, Kasman I, Zhang J, et al. An interleukin-17-mediated paracrine network promotes tumor resistance to anti-angiogenic therapy. Nat Med 2013 Sep;19(9):1114-1123.

(50) Coffelt SB, Wellenstein MD, de Visser KE. Neutrophils in cancer: neutral no more. Nat Rev Cancer 2016 Jul;16(7):431-446.

(51) Denny MF, Yalavarthi S, Zhao W, Thacker SG, Anderson M, Sandy AR, et al. A distinct subset of proinflammatory neutrophils isolated from patients with systemic lupus erythematosus induces vascular damage and synthesizes type I IFNs. J Immunol 2010 Mar 15;184(6):3284-3297.

(52) Pillay J, Kamp VM, van Hoffen E, Visser T, Tak T, Lammers JW, et al. A subset of neutrophils in human systemic inflammation inhibits T cell responses through Mac-1. J Clin Invest 2012 Jan;122(1):327-336.

(53) Ueda Y, Cain DW, Kuraoka M, Kondo M, Kelsoe G. IL-1R type I-dependent hemopoietic stem cell proliferation is necessary for inflammatory granulopoiesis and reactive neutrophilia. J Immunol 2009 May 15;182(10):6477-6484.

(54) Mankan AK, Canli O, Schwitalla S, Ziegler P, Tschopp J, Korn T, et al. TNF-alpha-dependent loss of IKKbeta-deficient myeloid progenitors triggers a cytokine loop culminating in granulocytosis. Proc Natl Acad Sci U S A 2011 Apr 19;108(16):6567-6572.

(55) Kim MH, Granick JL, Kwok C, Walker NJ, Borjesson DL, Curry FR, et al. Neutrophil survival and c-kit(+)-progenitor proliferation in staphylococcus aureus-infected skin wounds promote resolution. Blood 2011 Mar 24;117(12):3343-3352.

(56) Pillay J, Ramakers BP, Kamp VM, Loi AL, Lam SW, Hietbrink F, et al. Functional heterogeneity and differential priming of circulating neutrophils in human experimental endotoxemia. J Leukoc Biol 2010 Jul;88(1):211-220.

(57) Tsuda Y, Takahashi H, Kobayashi M, Hanafusa T, Herndon DN, Suzuki F. Three different neutrophil subsets exhibited in mice with different susceptibilities to infection by methicillin-resistant staphylococcus aureus. Immunity 2004 Aug;21(2):215-226.

(58) Casbon AJ, Reynaud D, Park C, Khuc E, Gan DD, Schepers K, et al. Invasive breast cancer reprograms early myeloid differentiation in the bone marrow to generate immunosuppressive neutrophils. Proc Natl Acad Sci U S A 2015 Feb 10;112(6):E566-75.

(59) Coffelt SB, Kersten K, Doornebal CW, Weiden J, Vrijland K, Hau CS, et al. IL-17-producing γδ T cells and neutrophils conspire to promote breast cancer metastasis. Nature 2015 Jun 18;522(7556):345-348.

(60) Panopoulos AD, Zhang L, Snow JW, Jones DM, Smith AM, El Kasmi KC, et al. STAT3 governs distinct pathways in emergency granulopoiesis and mature neutrophils. Blood 2006 Dec 1;108(12):3682-3690.

(61) Sawanobori Y, Ueha S, Kurachi M, Shimaoka T, Talmadge JE, Abe J, et al. Chemokine-mediated rapid turnover of myeloid-derived suppressor cells in tumor-bearing mice. Blood 2008 Jun 15;111(12):5457-5466.

(62) Colotta F, Re F, Polentarutti N, Sozzani S, Mantovani A. Modulation of granulocyte survival and programmed cell death by cytokines and bacterial products. Blood 1992 Oct 15;80(8):2012-2020.

(63) Steinbach KH, Schick P, Trepel F, Raffler H, Döhrmann J, Heilgeist G, et al. Estimation of kinetic parameters of neutrophilic, eosinophilic, and basophilic granulocytes in human blood. Blut 1979 Jul;39(1):27-38.

(64) Valadez-Cosmes P, Maitz K, Kindler O, Raftopoulou S, Kienzl M, Santiso A, et al. Identification of novel low-density neutrophil markers through unbiased high-dimensional

flow cytometry screening in non-small cell lung cancer patients. Front Immunol 2021 Aug 13;12:703846.

(65) Häger M, Cowland JB, Borregaard N. Neutrophil granules in health and disease. J Intern Med 2010 Jul;268(1):25-34.

(66) Fridlender ZG, Sun J, Kim S, Kapoor V, Cheng G, Ling L, et al. Polarization of tumor-associated neutrophil phenotype by TGF-beta: "N1" versus "N2" TAN. Cancer Cell 2009 Sep 8;16(3):183-194.

(67) Ohms M, Möller S, Laskay T. An attempt to polarize human neutrophils toward N1 and N2 phenotypes in vitro. Front Immunol 2020 Apr 28;11:532.

(68) Mantovani A, Cassatella MA, Costantini C, Jaillon S. Neutrophils in the activation and regulation of innate and adaptive immunity. Nat Rev Immunol 2011 Jul 25;11(8):519-531.

(69) Faget J, Peters S, Quantin X, Meylan E, Bonnefoy N. Neutrophils in the era of immune checkpoint blockade. J Immunother Cancer 2021 Jul;9(7):e002242. doi: 10.1136/jitc-2020-002242.

(70) Antonio N, Bønnelykke-Behrndtz ML, Ward LC, Collin J, Christensen IJ, Steiniche T, et al. The wound inflammatory response exacerbates growth of pre-neoplastic cells and progression to cancer. EMBO J 2015 Sep 2;34(17):2219-2236.

(71) Deshmukh HS, Liu Y, Menkiti OR, Mei J, Dai N, O'Leary CE, et al. The microbiota regulates neutrophil homeostasis and host resistance to Escherichia coli K1 sepsis in neonatal mice. Nat Med 2014 May;20(5):524-530.

(72) Bodogai M, Moritoh K, Lee-Chang C, Hollander CM, Sherman-Baust CA, Wersto RP, et al. Immunosuppressive and prometastatic functions of myeloid-derived suppressive cells rely upon dducation from tumor-associated B cells. Cancer Res 2015 Sep 1;75(17):3456-3465.

(73) Houghton AM, Rzymkiewicz DM, Ji H, Gregory AD, Egea EE, Metz HE, et al. Neutrophil elastase-mediated degradation of IRS-1 accelerates lung tumor growth. Nat Med 2010 Feb;16(2):219-223.

(74) Nozawa H, Chiu C, Hanahan D. Infiltrating neutrophils mediate the initial angiogenic switch in a mouse model of multistage carcinogenesis. Proc Natl Acad Sci U S A 2006 Aug 15;103(33):12493-12498.

(75) Yang L, DeBusk LM, Fukuda K, Fingleton B, Green-Jarvis B, Shyr Y, et al. Expansion of myeloid immune suppressor Gr+CD11b+ cells in tumor-bearing host directly promotes tumor angiogenesis. Cancer Cell 2004 Oct;6(4):409-421.

(76) Coussens LM, Tinkle CL, Hanahan D, Werb Z. MMP-9 supplied by bone marrow-derived cells contributes to skin carcinogenesis. Cell 2000 Oct 27;103(3):481-490.

(77) Shojaei F, Singh M, Thompson JD, Ferrara N. Role of Bv8 in neutrophil-dependent angiogenesis in a transgenic model of cancer progression. Proc Natl Acad Sci U S A 2008 Feb 19;105(7):2640-2645.

(78) Shojaei F, Wu X, Zhong C, Yu L, Liang XH, Yao J, et al. Bv8 regulates myeloid-cell-dependent tumour angiogenesis. Nature 2007 Dec 6;450(7171):825-831.

(79) Tazzyman S, Niaz H, Murdoch C. Neutrophil-mediated tumour angiogenesis: subversion of immune responses to promote tumour growth. Semin Cancer Biol 2013 Jun;23(3):149-158.

(80) Catena R, Bhattacharya N, El Rayes T, Wang S, Choi H, Gao D, et al. Bone marrow-derived Gr1+ cells can generate a metastasis-resistant microenvironment via induced secretion of thrombospondin-1. Cancer Discov 2013 May;3(5):578-589.

(81) Kaplan RN, Riba RD, Zacharoulis S, Bramley AH, Vincent L, Costa C, et al. VEGFR1-positive haematopoietic bone marrow progenitors initiate the pre-metastatic niche. Nature 2005 Dec 8;438(7069):820-827.

(82) Hiratsuka S, Nakamura K, Iwai S, Murakami M, Itoh T, Kijima H, et al. MMP9 induction by vascular endothelial growth factor receptor-1 is involved in lung-specific metastasis. Cancer Cell 2002 Oct;2(4):289-300.

(83) Bertini R, Allegretti M, Bizzarri C, Moriconi A, Locati M, Zampella G, et al. Noncompetitive allosteric inhibitors of the inflammatory chemokine receptors CXCR1 and CXCR2: prevention of reperfusion injury. Proc Natl Acad Sci U S A 2004 Aug 10;101(32):11791-11796.

(84) Eruslanov EB, Bhojnagarwala PS, Quatromoni JG, Stephen TL, Ranganathan A, Deshpande C, et al. Tumor-associated neutrophils stimulate T cell responses in early-stage human lung cancer. J Clin Invest 2014 Dec;124(12):5466-5480.

(85) ClinicalTrials.gov. Phase Ib of L-NMMA and pembrolizumab. 2022; Available at: https://clinicaltrials.gov/ct2/show/NCT03236935. Accessed Apr/2022.

(86) ClinicalTrials.gov. Arginase inhibitor INCB001158 as a single agent and in combination with immune checkpoint therapy in patients with advanced/metastatic solid tumors. 2022; Available at: https://clinicaltrials.gov/ct2/show/NCT02903914?term=INCB001158&type=Intr&cond=NSCLC&cntry=US&draw=2&rank=2. Accessed Apr/2022.

(87) ClinicalTrials.gov. Grapiprant (ARY-007) and pembrolizumab in patients with advanced or metastatic post-PD-1/L1 NSCLC adenocarcinoma. 2022; Available at: https://clinicaltrials.gov/ct2/show/NCT03696212?term=grapiprant&type=Intr&cond=NSCLC&cntry=US&draw=2&rank=1. Accessed Apr/2022.

(88) Shojaei F, Wu X, Malik AK, Zhong C, Baldwin ME, Schanz S, et al. Tumor refractoriness to anti-VEGF treatment is mediated by CD11b+Gr1+ myeloid cells. Nat Biotechnol 2007 Aug;25(8):911-920.

(89) Phan VT, Wu X, Cheng JH, Sheng RX, Chung AS, Zhuang G, et al. Oncogenic RAS pathway activation promotes resistance to anti-VEGF therapy through G-CSF-induced neutrophil recruitment. Proc Natl Acad Sci U S A 2013 Apr 9;110(15):6079-6084.

(90) Kersten K, Salvagno C, de Visser KE. Exploiting the immunomodulatory properties of chemotherapeutic drugs to improve the success of cancer immunotherapy. Front Immunol 2015 Oct 7;6:516.

(91) Di Maio M, Gridelli C, Gallo C, Shepherd F, Piantedosi FV, Cigolari S, et al. Chemotherapy-induced neutropenia and treatment efficacy in advanced non-small-cell lung cancer: a pooled analysis of three randomised trials. Lancet Oncol 2005 Sep;6(9):669-677.

(92) Han Y, Yu Z, Wen S, Zhang B, Cao X, Wang X. Prognostic value of chemotherapy-induced neutropenia in early-stage breast cancer. Breast Cancer Res Treat 2012 Jan;131(2):483-490.

(93) Yamanaka T, Matsumoto S, Teramukai S, Ishiwata R, Nagai Y, Fukushima M. Predictive value of chemotherapy-induced neutropenia for the efficacy of oral fluoropyrimidine S-1 in advanced gastric carcinoma. Br J Cancer 2007 Jul 2;97(1):37-42.

(94) Shitara K, Matsuo K, Takahari D, Yokota T, Inaba Y, Yamaura H, et al. Neutropaenia as a prognostic factor in metastatic colorectal cancer patients undergoing chemotherapy with first-line FOLFOX. Eur J Cancer 2009 Jul;45(10):1757-1763.

(95) Cossarizza A, Chang HD, Radbruch A, Acs A, Adam D, Adam-Klages Sea. Guidelines for the use of flow cytometry and cell sorting in immunological studies (second edition). Eur J Immunol 2019 Oct;49(10):1457-1973.

(96) Lückerath K, Hildmann J. Introduction into flow cytometry by BD Biosciences, customer service. Available at: https://www.biochem.uni-frankfurt.de/fileadmin/user_upload/courses_practicals/BCII_GSH_Vortrag07.pdf. Accessed Oct/2021.

(97) Depince-Berger AE, Aanei C, Iobagiu C, Jeraiby M, Lambert C. New tools in cytometry. Morphologie 2016 Dec;100(331):199-209.

(98) BD Biosciences. FlowJo(R) basic tutorial version 2.0. 2018; Available at: https://cdn2.hubspot.net/hubfs/2566672/Sales%20Documents/FlowJo%C2%AE_Basic_Tutorial_%C2%A92018.pdf. Accessed Nov/2021.

(99) Zeilinger M, Hübl W. Durchflusszytometrie - eine Einführung. Feb/2006; Available at: https://www.med4you.at/laborbefunde/techniken/durchflusszytometrie/lbef_durchflusszytometrie.htm#Gaten. Accessed Oct/2021.

(100) Rotondo R, Barisione G, Mastracci L, Grossi F, Orengo AM, Costa R, et al. IL-8 induces exocytosis of arginase 1 by neutrophil polymorphonuclears in nonsmall cell lung cancer. Int J Cancer 2009 Aug 15;125(4):887-893.

(101) Kargl J, Zhu X, Zhang H, Yang GHY, Friesen TJ, Shipley M, et al. Neutrophil content predicts lymphocyte depletion and anti-PD1 treatment failure in NSCLC. JCI Insight 2019 Dec 19;4(24):e130850. doi: 10.1172/jci.insight.130850.

(102) Sagiv JY, Michaeli J, Assi S, Mishalian I, Kisos H, Levy L, et al. Phenotypic diversity and plasticity in circulating neutrophil subpopulations in cancer. Cell Rep 2015 Feb 3;10(4):562-573.

(103) Ilie M, Hofman V, Ortholan C, Bonnetaud C, Coëlle C, Mouroux J, et al. Predictive clinical outcome of the intratumoral CD66b-positive neutrophil-to-CD8-positive T-cell ratio in patients with resectable nonsmall cell lung cancer. Cancer 2012 Mar 15;118(6):1726-1737.

(104) Templeton AJ, McNamara MG, Šeruga B, Vera-Badillo FE, Aneja P, Ocaña A, et al. Prognostic role of neutrophil-to-lymphocyte ratio in solid tumors: a systematic review and meta-analysis. J Natl Cancer Inst 2014 May 29;106(6):dju124.

(105) Fridlender ZG, Albelda SM. Tumor-associated neutrophils: friend or foe? Carcinogenesis 2012 May;33(5):949-955.

(106) Moses K, Brandau S. Human neutrophils: Their role in cancer and relation to myeloid-derived suppressor cells. Semin Immunol 2016 Apr;28(2):187-196.

(107) Youn JI, Nagaraj S, Collazo M, Gabrilovich DI. Subsets of myeloid-derived suppressor cells in tumor-bearing mice. J Immunol 2008 Oct 15;181(8):5791-5802.

(108) Koyama S, Akbay EA, Li YY, Aref AR, Skoulidis F, Herter-Sprie GS, et al. STK11/LKB1 Deficiency Promotes Neutrophil Recruitment and Proinflammatory Cytokine Production to Suppress T-cell Activity in the Lung Tumor Microenvironment. Cancer Res 2016 Mar 1;76(5):999-1008.

(109) STEMCELL Technologies. Directions for use - Manual EasySep™ protocols. 2021; Available at: https://cdn.stemcell.com/media/files/pis/10000005298-PIS_01.pdf?_ga=2.27606393.450466575.1636465549-899028909.1636107714. Accessed Nov/2021.

(110) Ethier C. Vitamin D, an immunomodulator for eosinophils in asthma and allergy (picture of Kimuras formula). Aug/2014; Available at: https://www.researchgate.net/figure/Kimura-stain-formulation-and-specific-functions_tbl2_274698312. Accessed Jan/2022.

(111) LO Laboroptik GmbH. Zählkammer Neubauer - improved. Available at: http://zaehlkammer.de/deutsch/neubauer.improved.html. Accessed Oct/2021.

(112) Bioanalytik GmbH. Produktinformation, Neubauer Zählkammer. 2019; Available at: https://www.bioanalytic.de/en/product/article/neubauer-improved-420.html?file=files/bioanalytic/downloads/Produktinformationen/bioanalytic/bioPIN%20CountingChamber%20MULTIUSE%20-%20bioanalytic%20%28de%29.pdf. Accessed Oct/2021.

(113) Miltenyi Biotec. Eosinophil isolation kit, human (data sheet). 2021; Available at: https://www.miltenyibiotec.com/upload/assets/IM0001390.PDF. Accessed Nov/2021.

(114) Miltenyi Biotec. MACS(R) Columns for magnetic cell isolation. 2021; Available at: https://www.miltenyibiotec.com/AT-en/products/macs-cell-separation/columns/macs-columns-at-a-glance.html?countryRedirected=1#gref. Accessed Nov/2021.

(115) Schratl P, Heinemann A. Differential involvement of Ca2+ and actin filament in leukocyte shape change. Pharmacology 2009;83(3):131-140.

(116) Han X, Na T, Wu T, Yuan B. Human lung epithelial BEAS-2B cells exhibit characteristics of mesenchymal stem cells. PLoS ONE January 3, 2020;15(1): e0227174.

(117) Foster KA, Oster CG, Mayer MM, Avery ML, Audus KL. Characterization of the A549 cell line as a type II pulmonary epithelial cell model for drug metabolism. Exp Cell Res 1998 15 September 1998;243(2):359-366.

(118) American Type Culture Collection (ATCC). A549 product sheet. 2022; Available at: https://www.atcc.org/atcc/productsheetpdf/generatehtmlpdf/crm-ccl-185. Accessed Apr/2022.

(119) American Type Culture Collection (ATCC). BEAS-2B product sheet. 2022; Available at: https://www.atcc.org/atcc/productsheetpdf/generatehtmlpdf/crl-9609. Accessed Apr/2022.

(120) Kienzl M, Hasenoehrl C, Valadez-Cosmes P, Maitz K, Sarsembayeva A, Sturm E, et al. IL-33 reduces tumor growth in models of colorectal cancer with the help of eosinophils. Oncoimmunology 2020 Jun 16;9(1):1776059.

(121) Kienzl M, Hasenoehrl C, Maitz K, Sarsembayeva A, Taschler U, Valadez-Cosmes P, et al. Monoacylglycerol lipase deficiency in the tumor microenvironment slows tumor growth in non-small cell lung cancer. Oncoimmunology 2021 Sep 11;10(1):1965319.

(122) BD Biosciences. FITC annexin V apoptosis detection kit I, technical data sheet. 2021; Available at: https://www.bdbiosciences.com/en-us/products/reagents/flow-cytometry-reagents/research-reagents/panels-multicolor-cocktails-ruo/fitc-annexin-v-apoptosis-detection-kit-i.556547. Accessed Nov/2021.

(123) BD Biosciences. BD FACSCanto II flow cytometer, technical specifications. 2009; Available at: https://www.bdbiosciences.com/content/dam/bdb/marketing-documents/facscanto_techspecs.pdf. Accessed Oct/2021.

(124) Finak G, Langweiler M, Jaimes M, Malek M, Taghiyar J, Korin Yea. Standardizing flow cytometry immunophenotyping analysis from the Human ImmunoPhenotyping Consortium. Sci Rep 2016 Feb 10;6:20686.

(125) Thermo Fisher Scientific Inc. eBioscience(TM) cell proliferation dye eFluor(TM) 450, technical data sheet. Jan/2021; Available at: https://www.thermofisher.com/document-connect/document-

connect.html?url=https://assets.thermofisher.com/TFS-Assets%2FLSG%2Fmanuals%2F65-0842.pdf. Accessed Nov/2021.

(126) BioLegend Inc. Human TruStain FcX(TM), Fc receptor blocking solution, technical data sheet. Jul/2016; Available at: https://www.biolegend.com/en-us/global-elements/pdf-popup/human-trustain-fcx-fc-receptor-blocking-solution-6462?filename=Human TruStain FcXtrade Fc Receptor Blocking Solution.pdf&pdfgen=true. Accessed Nov/2021.

(127) Thermo Fisher Scientific Inc. eBioscience(TM) fixable viability dye eFluor(TM) 780, technical data sheet. Jan/2017; Available at: https://www.thermofisher.com/document-connect/document-connect.html?url=https%3A%2F%2Fassets.thermofisher.com%2FTFS-Assets%2FLSG%2Fmanuals%2F65-0865.pdf. Accessed Nov/2021.

(128) BD Biosciences. BD FACSCanto II, instructions for use. 2007; Available at: https://pedsresearch.org/_files/BD_FACS_Canto_II_Users_Guide.pdf. Accessed Nov/2021.

(129) BD Biosciences. Lasers and dyes. 2021; Available at: https://www.bdbiosciences.com/en-at/learn/applications/multicolor-flow-cytometry/lasers-and-dyes#overview. Accessed Nov/2021.

(130) Thermo Fisher Scientific Inc. Fluorophore selection. 2021; Available at: https://www.thermofisher.com/at/en/home/life-science/cell-analysis/fluorophores.html. Accessed Nov/2021.

(131) Trinity Biomedical Sciences Institute. Fluorochrome list. 2014; Available at: https://www.tcd.ie/Biochemistry/assets/pdfs/Fluorochrome_List_2014.pdf. Accessed Nov/2021.

(132) BioLegend Inc. The stain index: what is it and what does it tell you? 2021; Available at: https://www.biolegend.com/en-us/blog/the-stain-index-what-is-it-and-what-does-it-tell-you. Accessed Oct/2021.

(133) FluoroFinder. Newsletter: staining index. May/2019; Available at: https://fluorofinder.com/newsletter-staining-index/. Accessed Oct/2021.

(134) Roederer M. Compensation: an informal perspective. Apr/2013; Available at: http://www.drmr.com/. Accessed Oct/2021.

(135) Zeilinger M, Hübl W. Durchflusszytometrie - Einführung in die Kompensation. Jun/2006; Available at: https://www.med4you.at/laborbefunde/techniken/durchflusszytometrie/lbef_durchflusszytometrie_kompensation.htm. Accessed Oct/2021.

(136) Thermo Fisher Scientific Inc. Fluorescence SpectraViewer. 2021; Available at: https://www.thermofisher.com/order/fluorescence-spectraviewer?gclid=CjwKCAiAvriMBhAuEiwA8Cs5laz-f3dvZeNMwDnZil6633OxR7PvPS03eDE6VcrWQVfTJ4PiCRpngBoC5x0QAvD_BwE&ef_id=CjwKCAiAvriMBhAuEiwA8Cs5laz-

f3dvZeNMwDnZil6633OxR7PvPS03eDE6VcrWQVfTJ4PiCRpngBoC5x0QAvD_BwE:G:s&s_kwcid=AL!3652!3!546509333980!e!!g!!thermo%20fisher%20spectra%20viewer&cid=bid_pca_aup_r01_co_cp1359_pjt0000_bid00000_0se_gaw_bt_pur_con#!/. Accessed Nov/2021.

(137) Garley M, Jabłońska E. Heterogeneity Among Neutrophils. Arch Immunol Ther Exp (Warsz) 2018 Feb;66(1):21-30.